Article:
Shen, Q., Liu, W., Wang, L. et al. (2020) Group sparsity based localization for far-field and near-field sources based on distributed sensor array networks. IEEE Transactions on Signal Processing, 68. pp. 6493-6508. ISSN: 1053-587X

https://doi.org/10.1109/TSP.2020.3037841

Group Sparsity Based Localization for Far-Field and Near-Field Sources Based on Distributed Sensor Array Networks

Qing Shen, Wei Liu, *Senior Member, IEEE,* Li Wang, and Yin Liu

***Abstract*—A distributed sensor array network is studied, where sub-arrays are placed on those distributed observation platforms. In this model, bearing-only source localization is characterized in terms of direction of arrival (DOA) if the sources are far from the entire network, while their locations in the predefined Cartesian coordinate system can be obtained for the near-field case. For wideband signals, the focusing algorithm is applied at each sub-array to form an equivalent single frequency signal model. Then, a compressive sensing (CS) based DOA estimation method employing the group sparsity concept is proposed for far-field sources with the information acquired by all the platforms processed as a whole. This concept is further extended to near field, and a group sparsity based method to localize the near-field sources is derived. The proposed solutions are applicable for both uncorrelated and coherent signals, and the corresponding Cramér-Rao Bounds (CRBs) are derived. Compared with the maximum likelihood estimator (MLE) of forming the final result through a fusion process, where separately estimated unreliable bearing result at even one observation platform would spoil the overall performance, improved performance is achieved by both proposed methods. It is noted that only the covariance matrix in lieu of data samples at each platform is required for centralized processing, and therefore the increase of the data exchange workload among platforms is rather limited.**

***Index Terms*—Distributed sensor array network, group sparsity, localization, far-field and near-field sources, narrowband and wideband.**

I. Introduction

Source localization based on various sensor array networks has attracted significant attentions over the past decade [2]–[4]. Apart from some notable localization techniques based on received signal strength (RSS) [5] and distance related measurements such as time of arrival (TOA) [6], the angle of arrival (AOA) based source localization, also known as direction of arrival (DOA) based localization or bearing-only localization, is an attractive candidate since the synchronization among the distributed platforms is not required [7], and it can be used in both active and passive sensing networks.

Part of this work was presented at the 2019 IEEE International Conference on Acoustics, Speech, and Signal Processing (ICASSP), Brighton, UK [1]. This work was supported in part by the National Natural Science Foundation of China under Grants 61801028 and 61628101 and the U.K. Engineering and Physical Sciences Research Council (EPSRC) under Grant EP/T517215/1.

Q. Shen is with the School of Information and Electronics, Beijing Institute of Technology, Beijing, 100081, China (e-mail: qing-shen@outlook.com).

W. Liu is with the Department of Electronic and Electrical Engineering, University of Sheffield, Sheffield, S1 3JD, UK (e-mail: w.liu@sheffield.ac.uk).

L. Wang and Y. Liu are with the Southwest China Institute of Electronic Technology, Chengdu, 610036, China; L. Wang is also with the School of Electronics and Information Engineering, Sichuan University, China.

The AOA based approach has been adopted in a wide range of applications including multistatic radar [2], [8], distributed massive MIMO [9], [10], and wireless sensor networks [11]. For far-field sources, AOA based approach can only be characterized in terms of DOA of the sources [12]–[14]. On the other hand, source locations can be uniquely determined in the Cartesian coordinate system for the near-field case [15]–[17].

There are normally two steps in AOA based localization: the incident angles are measured at all distributed observation platforms in the first step, followed by triangulation to locate the sources of interest in the second step. For each platform to estimate the AOA information, an array of sensors can be employed and many high-resolution methods can be applied here, such as the subspace-based ones including MUSIC [18], ESPRIT [19], and their extensions, while spatial smoothing is usually employed for preprocessing coherent signals [20].

In addition to those subspace-based methods, sparse signal representation, which is linked to the compressive sensing (CS) framework, is also introduced for DOA estimation [21]–[23]. A CS-based method for a single snapshot is presented in [24], while for multiple snapshots, the $\ell_{2,1}$ mixed norm is presented for the multiple measurement vectors (MMVs) scenario, and ℓ_1-SVD based on singular value decomposition (SVD) is proposed with the advantages of smaller number of data samples required and lower sensitivity to signal to noise ratio (SNR) [24]. DOA estimation method based on a sparse representation of array covariance vectors, referred to as ℓ_1-SRACV, is proposed in [25]. Both ℓ_1-SVD and ℓ_1-SRACV require reduced computational cost than the well-known $\ell_{2,1}$ mixed norm, and are capable of handling coherent signals. The theoretical guarantees for this joint sparse recovery problem from MMVs developed in [26] (the overdetermined case) and [27], [28] (the underdetermined case with sparse arrays and uncorrelated sources) are based on a fixed deterministic measurement matrix representing the steering matrix of an array structure, which deviates from usual scenarios in compressed sensing relying on the randomness of the measurement matrix, while the support recovery for both the deterministic and random measurement matrix is discussed in [29]. Based on the fundamental $\ell_{2,1}$ mixed norm, the MMV atomic norm approach [30] focusing mainly on the noiseless case and the SPARROW approach [31] are proposed as variants capable of incorporating the gridless optimization. However, in the noisy case and the small number of snapshots case, the covariance matrix of data samples is not guaranteed to be Toeplitz, and the matrix approximation after the necessary Vander-

monde decomposition may lead to performance degradation. In [32], the sparse spectrum fitting (SpSF) method for both uncorrelated sources (based on a vectorization process [33]) and coherent sources is proposed, and significant complexity reduction can be achieved if the sources are known *a priori* to be uncorrelated. The vectorization based methods [32], [33] (also commonly referred to as the co-array based methods) for prior-known uncorrelated sources are studied for the underdetermined case where the number of sources exceeds the number of physical sensors [34]–[39].

For wideband DOA estimation, the array received signals can be decomposed into a series of narrowband signals using the discrete Fourier transform (DFT), and some typical methods such as the incoherent signal subspace method (ISSM) [40], the coherent signal subspace method (CSSM) [41], and the test of orthogonality of projected subspaces (TOPS) method [42] can be employed. Under the CS framework, a more effective method, i.e., group sparsity based wideband DOA estimation method, is proposed in [43], [44], where the incident angles are estimated jointly across the frequencies of interest. To reduce the computational complexity, the focusing technique can be applied to the generated virtual array structure first, followed by CS-based DOA estimation [45], [46].

All the aforementioned DOA estimation methods are based on a single array structure (either uniform or non-uniform arrays), where the array sensors are part of a whole centred system. For direction finding based on distributed sensor array networks with widely separated subarrays, it is beneficial to exploit the whole large aperture through coherent processing algorithms [47], [48]. However, the raw data samples are required at the processing center to compute the covariance matrix including the inter-subarray ones, and the resultant communication overhead at both subarray platforms and the processing center are extremely high. On the contrast, non-coherent DOA estimation methods [49]–[52] has attracted great attentions due to their significantly reduced communication cost. Although the performance of the non-coherent DOA estimation methods is inferior to that of coherent processing ones, the computational load and also the communication overhead are significantly reduced since only the DOA measurements or the covariance matrices at subarrays are utilized in the following fusion process [53], [54]. Moreover, the consensus propagation concept can be employed in distributed fusion strategy by fusing information from neighborhood [55]–[57], and thus low communication overhead is feasible and the final fusion center is no longer needed. Recently, the sparse signal representation method (extended SPICE) based on covariance matrices at subarrays was introduced as a solution to partly calibrated sensor arrays [58] with Cramér-Rao Bound (CRB) derived, but the statistical properties of the observed signals at different subarrays are assumed to be identical, which may not be satisfied in practice especially for near-field source localization where the spatial diversity and different propagation attenuation cannot be ignored; for example, the equivalent source power after taking into propagation attenuation will be different for different subarrays and different subarrays could work on different frequencies; in the active sensing case, the radar cross section (RCS) or similar parameters of the targets may be different for different subarrays.

Source localization can also be achieved by a distributed sensor array network, where multiple sensors or sensor arrays are distributed in widely separated spatial locations and the DOA results obtained by each of them can then be combined together to obtain the location of the source across the distributed platforms when near-field sources are considered [4], [10], [59]. The maximum likelihood estimator (MLE) has been adopted to minimize the total errors of the noise-corrupted angle measurements among all distributed platforms under the least square sense [8], [60]. However, the angle measurements are nonlinearly related to source locations and the objective function is non-convex [3], [60], [61], leading to a difficult optimization problem. Instead of the time-consuming grid search method for the MLE, a number of low-complexity iterative methods can be employed [62], but their performance is sensitive to the initializations and a globally optimal solution cannot be obtained in many cases due to the non-convex objective function. To further reduce the complexity, some closed-form location estimators have also been proposed [7], [11], [63].

However, by using the maximum likelihood (ML) criteria to minimize the root mean square errors (RMSEs) of the angle measurements, the performance of the MLE is dependent on the angle measurements obtained at all platforms, and even one worse AOA estimation result at a certain platform can lead to serious performance degradation. How to further improve the estimation performance by processing the collected information across the observation platforms jointly in lieu of fusing the separately measured angle results at all platforms is still a challenge.

In this paper, we study the source localization problem for wideband signals based on a distributed sensor array network consisting of multiple receivers as in [64], where a linear subarray is placed on each observation platform. However, the proposed approach is also applicable to narrowband sources by simply removing the focusing part, as they can be considered as a special case.

In the first task, we focus on DOA estimation for far-field sources whose wave-fronts arriving at the distributed sensor array network can be considered as a plane. The propagation coefficients of the same source observed at different receivers may not be the same due to the different radial distances and relative movements, or the radar cross section (RCS) fluctuations in the active sensing case. For complexity reduction, the focusing algorithm is applied to deal with the wideband signals at each observation platform and a combined equivalent single frequency signal model can be obtained. An efficient CS-based method employing the group sparsity concept, which is applicable for both uncorrelated signals and coherent signals, is proposed to exploit all the acquired information across distributed sub-arrays jointly, leading to improved estimation performance compared with that of existing DOA estimation method based on a single receiver.

Then, we consider the case of relatively near-field sources compared to the entire distributed sensor array network, while the sources are still far-field compared to each sub-array aperture. For a given source, there is a unique incident angle

observed at each sub-array, and it is possible to localize the source by enforcing common sparsity for all receivers in the predefined Cartesian coordinate system, leading to our proposed solution for localization of near-field sources based on the focused signal models. Instead of fusing the independent DOA estimation results provided by all receivers and then form a final localization result of the sources, the proposed solution is able to exploit the information collected by all the sub-arrays in the whole network, offering better performance than the MLE through fusing the pre-processed AOA results at all platforms. Moreover, one advantage associated with the aforementioned solutions is that, only the covariance matrix at each sub-array in lieu of all the data samples is required for centralized processing, and therefore the increase of the data exchange workload among platforms is limited compared with those AOA-based fusion methods.

The main contribution in this work is to present a general group-sparsity based approach capable of handling narrowband/wideband, far-field/near-field, and uncorrelated/coherent sources with potential frequency and spatial diversity, which are not fully considered in the literature. The proposed approach is flexible, as the different subarrays are not required to be synchronised and can work on different frequencies, the statistical properties of the sources can be different for different subarrays, and sensor numbers, rotation angles, and observed signals of different sub-arrays do not need to be the same. To our best knowledge, the proposed approach is the first one to be able to effectively deal with the above scenario in one step with closed-form CRB derived, in comparison with the two-step AOA-based fusion methods.

This paper is structured as follows. The considered distributed sensor array network is presented in Sec. II. The developed group sparsity based DOA estimation method for far-field sources is proposed in Sec. III, and the near-field case is dealt with in Sec. IV. The CRBs for both far-field and near-field cases are derived in Sec. V. Simulation results are provided in Sec. VI, and conclusions are drawn in Sec. VII.

II. System Model for Distributed Sensor Array Networks

A distributed sensor array network consisting of M sub-arrays with each fixed on a observation platform and K sources is shown in Fig. 1, where $\mathrm{U}_m(x_m, y_m)$ and $\mathrm{T}_k(x_{T_k}, y_{T_k})$ represent the locations of the m-th receiver and the k-th source in a predefined Cartesian coordinate system, respectively. The general array structure of the m-th receiver consisting of an L_m-sensor linear sub-array is shown in Fig. 2, and the sensor position set $\mathbb{S}_m$ of the sub-array is given as

$$\mathbb{S}_m = \{\hbar_l^m d,\ 0 \le l \le L_m - 1, l \in \mathbb{Z}\}\ , \tag{1}$$

where $\mathbb{Z}$ is the set of all integers, $\hbar_l^m d$ represents the position of the l-th sensor, and d is the unit spacing.

Assume that all the sources are far-field compared to each sub-array aperture, and $\phi_{m,k},\ m = 1, 2, \ldots, M,\ k = 1, 2, \ldots, K$, is the incident angle of the k-th source measured between the direction of the impinging signal on the m-th sub-array and the y-axis, given by

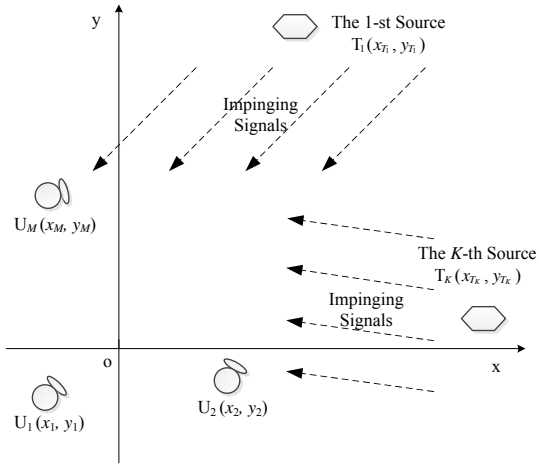

Fig. 1. A general model for a distributed sensor array network.

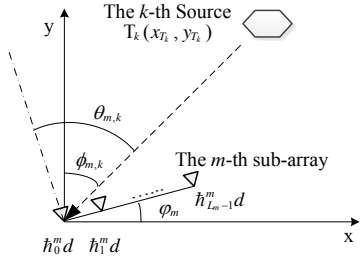

Fig. 2. A general array structure for the m-th sub-array carried by the corresponding observation platform.

$$\begin{aligned}\phi_{m,k} &= \arctan 2(\Delta x_{m,k}, \Delta y_{m,k}) \\ &= \begin{cases} \arctan(\frac{\Delta x_{m,k}}{\Delta y_{m,k}}), & \Delta y_{m,k} > 0, \\ \arctan(\frac{\Delta x_{m,k}}{\Delta y_{m,k}}) + \pi, & \Delta x_{m,k} \ge 0, \Delta y_{m,k} < 0, \\ \arctan(\frac{\Delta x_{m,k}}{\Delta y_{m,k}}) - \pi, & \Delta x_{m,k} < 0, \Delta y_{m,k} < 0, \\ +\frac{\pi}{2}, & \Delta x_{m,k} > 0, \Delta y_{m,k} = 0, \\ -\frac{\pi}{2}, & \Delta x_{m,k} < 0, \Delta y_{m,k} = 0, \\ \text{undefined}, & \Delta x_{m,k} = 0, \Delta y_{m,k} = 0, \end{cases} \end{aligned} \tag{2}$$

where $\arctan 2(a, b) \in (-\pi, \pi]$ represents the four-quadrant inverse tangent of a and b, with $\arctan(\frac{a}{b})$ being the inverse tangent of $\frac{a}{b}$, $\Delta x_{m,k} = x_{T_k} - x_m$, and $\Delta y_{m,k} = y_{T_k} - y_m$.

Denote $s_{m,k}(t)$ as the wideband signal received at the m-th sub-array, and φ_m is the rotation angle of the m-th receiver, measured between the end-fire direction of the linear sub-array and the x-axis. Then we have $\theta_{m,k} = \phi_{m,k} + \varphi_m$, with $\theta_{m,k}$ representing the incident angle of the impinging signal from the k-th source based on the m-th sub-array.

We use $\mathbf{x}_m(t)$ to represent the $L_m \times 1$ array observed signal vector, and the array output model at frequency f is given by

$$\mathbf{X}_m(f,t) = \mathbf{A}_m(f, \boldsymbol{\theta}_m)\mathbf{S}_m(f,t) + \overline{\mathbf{N}}_m(f,t)\ , \tag{3}$$

where $\mathbf{X}_m(f,t)$, $\mathbf{S}_m(f,t)$, and $\overline{\mathbf{N}}_m(f,t)$ are the components at frequency f regarding to $\mathbf{x}_m(t)$, the signal vector $\mathbf{s}_m(t)$, and the noise vector $\bar{\mathbf{n}}_m(t)$, respectively. The noises observed at different sensors are uncorrelated, and they are assumed to be white Gaussian and uncorrelated with the sources.

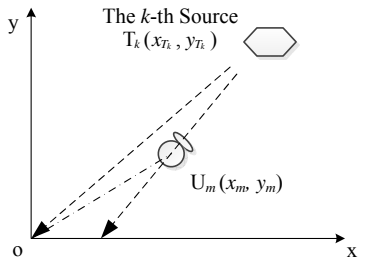

Fig. 3. The time delay.

$\mathbf{S}_m(f,t) = [b_{m,1}(f,t)S_{m,1}(f,t), \ldots, b_{m,K}(f,t)S_{m,K}(f,t)]^T$ consists of all the received signals at the sub-array, and $\{\cdot\}^T$ denotes the transpose operation. $b_{m,k}(f,t)$ is the propagation coefficient of the k-th source corresponding to the m-th sub-array which is related to the distance between the source and the platform, and may be time-varying due to relative motion between the source and the platform. In the active sensing network, $b_{m,k}(f,t)$ is also related to radar cross section (RCS) fluctuations incorporating spatial and frequency diversity. $\mathbf{A}_m(f,\boldsymbol{\theta}_m) = [\mathbf{a}_m(f,\theta_{m,1}), \mathbf{a}_m(f,\theta_{m,2}), \ldots, \mathbf{a}_m(f,\theta_{m,K})]$ is the $L_m \times K$ steering matrix, with its k-th column vector $\mathbf{a}(f,\theta_{m,k})$ being the steering vector corresponding to the k-th source, expressed as

$$\begin{aligned}&\mathbf{a}_m(f,\theta_{m,k})\\ =&\left[e^{-j\frac{2\pi\hbar_0^m d}{\lambda_f}\sin(\theta_{m,k})}, \ldots, e^{-j\frac{2\pi\hbar_{L_m-1}^m d}{\lambda_f}\sin(\theta_{m,k})}\right]^T ,\end{aligned} \tag{4}$$

with $\lambda_f = \frac{c}{f}$ and c being the wave propagation speed.

In the distributed sensor array network, the spacing between platforms is usually larger than the signal wavelength, and therefore for each frequency, the difference between those received signals across sub-arrays should be considered as a time delay instead of a phase shift in general. Define R_{AB} as the distance between positions A and B, and then the time delay between the m-th sub-array at U_m and the reference point at the origin $\mathrm{O}(0,0)$ (as shown in Fig. 3) is expressed as

$$\begin{aligned}\Delta\tau_{m,k} &= -\frac{R_{\mathrm{OT}_k} - R_{\mathrm{U}_m\mathrm{T}_k}}{c}\\ &= -\frac{\sqrt{x_{T_k}^2+y_{T_k}^2} - \sqrt{(x_{T_k}-x_m)^2+(y_{T_k}-t_m)^2}}{c} .\end{aligned} \tag{5}$$

Denote the signal observed at the origin $\mathrm{O}(0,0)$ as $s_{o,k}(t)$ with $S_{o,k}(f,t)$ representing its component at frequency f, $k = 1,2,\ldots,K$. Then, $\mathbf{S}_m(f,t)$ by taking $\mathrm{O}(0,0)$ as the reference is updated to

$$\begin{aligned}&\mathbf{S}_m(f,t)\\ =&[b_{m,1}(f,t)S_{m,1}(f,t), \ldots, b_{m,K}(f,t)S_{m,K}(f,t)]^T ,\end{aligned} \tag{6}$$

where

$$S_{m,k}(f,t) = S_{o,k}(f, t-\Delta\tau_{m,k}) . \tag{7}$$

Furthermore, denote the set of incident angles in the Cartesian coordinate system as $\boldsymbol{\phi}_k = \{\phi_{m,k}, m = 1,2,\ldots,M\}$. If $\max(\boldsymbol{\phi}_k) - \min(\boldsymbol{\phi}_k)$ is small enough (the appropriate bound would be related to the maximum tolerable error in applications), with $\max(\cdot)$ returning the maximum value of the input arguments and $\min(\cdot)$ giving the minimum one, the source will be considered as a far-field one compared with the distributed sensor array network, and we have $\phi_k \approx \phi_{m,k}$, $\forall m = 1,2,\ldots,M$. In practice, with the region of interest known, the geometric dilution of precision (GDOP) is helpful to decide which method (DOA estimation for far-field sources or localization for near-field sources) should be applied, and also useful for maintaining good layout of the platforms in the network [65]. Usually, for source localization in the distributed sensor array networks, *a priori* knowledge of the problem falling into either the far-field case or the near-field is needed before applying the appropriate method, with the aid of the known possible spatial area of interest of the targets; otherwise, a reasonable choice is to apply localization first and then DOA estimation if it fails [12].

III. DOA Estimation for Far-Field Sources

In this section, we consider far-field sources with all $\phi_{m,k}$, $m = 1,2,\ldots,M$, approximately the same, i.e., $\phi_k \approx \phi_{m,k}$. This problem is the same as the non-coherent DOA estimation with fully/partly calibrated subarrays [12], [49]–[52], and a global optimum can be obtained without ambiguous solutions. However, since the sensor numbers, the rotation angles, and the observed signals of different sub-arrays may not be the same, the signal models at different sub-arrays cannot be combined in a straightforward way. The uniqueness of the DOAs can be guaranteed due to the same $\phi_{m,k}$ to be estimated across subarrays by forcing the same spatial support within the incident angle range of interest.

A. Focusing for the Wideband Case

For the wideband case where the received signals share the same bandwidth, we first divide those received signals after sampling (with a sampling frequency f_s) into P non-overlapping groups with their length fixed at L, and then an L-point discrete Fourier transform (DFT) is applied to obtain the wideband array signal model, given as

$$\mathbf{X}_m[l,p] = \mathbf{A}_m(l,\boldsymbol{\theta})\mathbf{S}_m[l,p] + \overline{\mathbf{N}}_m[l,p] , \tag{8}$$

with the l_m-th entry in $\mathbf{X}_m[l,p]$, $\mathbf{S}_m[l,p]$, and $\overline{\mathbf{N}}_m[l,p]$ as

$$\begin{aligned}X_{m,l_m}[l,p] &= \sum\nolimits_{i=0}^{L-1} x_{m,l_m}[L\cdot(p-1)+i]\cdot e^{-j\frac{2\pi}{L}il} ,\\ S_{m,l_m}[l,p] &= \sum\nolimits_{i=0}^{L-1} s_{m,l_m}[L\cdot(p-1)+i]\cdot e^{-j\frac{2\pi}{L}il} ,\\ \overline{N}_{m,l_m}[l,p] &= \sum\nolimits_{i=0}^{L-1} \bar{n}_{m,l_m}[L\cdot(p-1)+i]\cdot e^{-j\frac{2\pi}{L}il} ,\end{aligned}$$

where for the m-th sub-array, $\mathbf{X}_m[l,p]$, $\mathbf{S}_m[l,p]$, and $\overline{\mathbf{N}}_m[l,p]$ represent the DFT of $\mathbf{x}_m[i]$, $\mathbf{s}_m[i]$, and $\bar{\mathbf{n}}_m[i]$ at the l-th frequency bin and the p-th group ($l = 0,1,\ldots,L-1$, $p = 1,2,\ldots,P$). $\mathbf{A}_m(l,\boldsymbol{\theta}) = [\mathbf{a}_m(l,\theta_{m,1}), \ldots, \mathbf{a}_m(l,\theta_{m,K})]$ is the steering matrix at $f_l = \frac{l}{L}f_s$ corresponding to the l-th frequency bin, with each column vector $\mathbf{a}_m(l,\theta_{m,k})$ the same as (4) except for a replacement of f by f_l.

The focusing algorithm [45] can be adopted to deal with the wideband signals. Denote f_r (corresponding to the l_r-th frequency bin) as the reference frequency for focusing, and the rotational signal-subspace (RSS) focusing matrix $\mathbf{T}_m[l]$ of the

m-th sub-array can be obtained by optimizing the following problem [45], [66]:

$$\begin{aligned} \min_{\mathbf{T}_m[l]} \quad & \|\mathbf{A}_m(l_r,\boldsymbol{\theta_F}) - \mathbf{T}_m[l]\mathbf{A}_m(l,\boldsymbol{\theta_F})\|_F \\ \text{subject to} \quad & \mathbf{T}_m^H[l]\mathbf{T}_m[l] = \mathbf{I}_{L_m} \ , \end{aligned} \tag{9}$$

and thus we have

$$\mathbf{T}_m[l] = \mathbf{V}_m[l]\mathbf{U}_m^H[l] \ , \tag{10}$$

where $\boldsymbol{\theta_F}$ holds the angles involved for focusing, $\|\cdot\|_F$ denotes the Frobenius norm, $\{\cdot\}^H$ denotes the Hermitian transpose, and $\mathbf{I}_{L_m}$ is the $L_m \times L_m$ identity matrix. The column vectors in $\mathbf{U}_m[l]$ and $\mathbf{V}_m[l]$ are the left and right singular vectors of the matrix $\mathbf{A}_m(l,\boldsymbol{\theta_F})\mathbf{A}_m{}^H(l_r,\boldsymbol{\theta_F})$, respectively.

Then, for the m-th sub-array, the focused array model at the l-th frequency bin is obtained by

$$\begin{aligned} \mathbf{y}_m[l,p] &= \mathbf{T}_m[l]\mathbf{X}_m[l,p] \\ &= \mathbf{T}_m[l]\mathbf{A}_m(l,\boldsymbol{\theta})\mathbf{S}_m[l,p] + \mathbf{T}_m[l]\overline{\mathbf{N}}_m[l,p] \\ &\approx \mathbf{A}_m(l_r,\boldsymbol{\theta})\mathbf{S}_m[l,p] + \mathbf{T}_m[l]\overline{\mathbf{N}}_m[l,p] \ . \end{aligned} \tag{11}$$

Assume that there are J frequency bins of interest with index l_j, $j = 0, 1, \ldots, J-1$. We can combine the array models at different frequencies of interest into a equivalent model at frequency f_r, given by

$$\begin{aligned} \bar{\mathbf{y}}_m[p] &= \sum\nolimits_{j=0}^{J-1} \mathbf{y}_m[l_j,p] \\ &= \mathbf{A}_m(l_r,\boldsymbol{\theta})\mathbf{u}_m[p] + \sum\nolimits_{j=0}^{J-1} \mathbf{T}_m[l_j]\overline{\mathbf{N}}_m[l_j,p] \ , \end{aligned} \tag{12}$$

where $\mathbf{u}_m[p] = \sum_{j=0}^{J-1} \mathbf{S}_m[l_j,p]$ is the $L_m \times 1$ equivalent signal vector.

Remark 1: For the wideband case, the group sparsity based method [43] can also be adopted and then extended to estimate the DOAs of far-field sources and localize the positions of near-field sources. However, its high computational complexity would be problematic when processing the information across multiple platforms.

B. The Optimal Choice of the Focusing Frequency

In [41], [66], the center frequency of the source spectrum is suggested to be the focusing frequency, and unitary focusing matrices are advocated. It has been proved that unbiased DOA estimates can be obtained for a single source scenario with the central frequency bin chosen as the focusing frequency [67]. For the multi-source scenario, the criterion of minimizing the subspace fitting error can be employed for focusing frequency selection [68]. The subspace fitting error (focusing error) is defined as

$$\begin{aligned} C(l_r) &= \frac{1}{P}\sum_{m=1}^{M}\sum_{j=0}^{J-1} \|\mathbf{Q}_m(l_r,l_j,\boldsymbol{\theta_F})\cdot\mathbf{S}_m[l_j]\|_F^2 \\ &= \sum_{m=1}^{M}\sum_{j=0}^{J-1} \mathrm{tr}\left\{\mathbf{Q}_m(l_r,l_j,\boldsymbol{\theta_F})\mathbf{R}_{\mathbf{S}_m}[l_j]\mathbf{Q}_m^H(l_r,l_j,\boldsymbol{\theta_F})\right\} \ , \end{aligned} \tag{13}$$

where $\mathbf{S}_m[l_j] = [\mathbf{S}_m[l_j,1],\ldots,\mathbf{S}_m[l_j,P]]$, $\mathbf{Q}_m(l_r,l_j,\boldsymbol{\theta_F}) = \mathbf{A}_m(l_r,\boldsymbol{\theta_F}) - \mathbf{T}_m[l_j]\mathbf{A}_m(l_j,\boldsymbol{\theta_F})$, $\mathbf{R}_{\mathbf{S}_m}[l_j]$ is the covariance matrix of the source signals, and $\mathrm{tr}\{\cdot\}$ is the trace operator.

According to the submultiplicavity property (also known as the mutually consistency property) of the Frobenius matrix norm with $\|\mathbf{AB}\|_F \le \|\mathbf{A}\|_F\|\mathbf{B}\|_F$, we have

$$\begin{aligned} C(l_r) &\le \sum_{m=1}^{M}\sum_{j=0}^{J-1} \|\mathbf{Q}_m(l_r,l_j,\boldsymbol{\theta_F})\|_F^2 \cdot \frac{1}{P}\|\mathbf{S}_m[l_j]\|_F^2 \\ &= \sum_{m=1}^{M}\sum_{j=0}^{J-1} \|\mathbf{Q}_m(l_r,l_j,\boldsymbol{\theta_F})\|_F^2 \cdot \sum_{k=1}^{K}\sigma_{m,k}^2[l_j] \\ &= C_{\max}(l_r) \ , \end{aligned} \tag{14}$$

where $\sigma_{m,k}^2[l_j]$ is the k-th source power at the m-th sub-array and the l_j-th frequency bin, and $\frac{1}{P}\|\mathbf{S}_m[l_j]\|_F^2 = \frac{1}{P}\mathrm{tr}\{\mathbf{S}_m[l_j]\mathbf{S}_m^H[l_j]\} = \sum_{k=1}^{K}\sigma_k^2$.

The subspace fitting error is upper bounded by $C_{\max}(l_r)$, and it is related to the source powers. For uncorrelated sources with high input SNRs, $\sum_{k=1}^{K}\sigma_k^2$ can be estimated by $\frac{1}{L_m}\mathrm{tr}\{\mathbf{R}_{\mathbf{y}_m}[l_j]\}$ with $\mathbf{R}_{\mathbf{y}_m}[l_j]$ being the covariance matrix of $\mathbf{y}_m[l,p]$.

If the source spectrums are known *a priori*, then the optimal focusing frequency can be obtained by solving the following optimization problem:

$$\min_{l_r} \quad C_{\max}(l_r) \quad \text{subject to} \quad \mathbf{A}_m(l_r,\boldsymbol{\theta_F}) \in \mathcal{A}(\boldsymbol{\theta_F}) \ , \tag{15}$$

with $\mathcal{A}(\boldsymbol{\theta_F}) = \{\mathbf{A}_m(l_j,\boldsymbol{\theta_F}) \mid j = 0,1,\ldots,J-1\}$ being the set of all steering matrices of interest for the focusing angles.

Consider the cases where all the source spectrums are identical with known distributions (although the exact received source powers at subarrays are unknown), only the normalized weights $w[l_j]$ proportional to the signal powers at different frequencies are of interest for solving (15), with $\sum_{j=0}^{J-1} w[l_j] = 1$ and $\sum_{k=1}^{K}\sigma_{m,k}^2[l_j]$ replaced by $w[l_j]$.

C. DOA Estimation Based on Sparse Representation of Array Covariance Vectors for a Single Sub-Array

Based on the focused model in (12), the covariance matrix is obtained by

$$\begin{aligned} \mathbf{R}_{\bar{\mathbf{y}}_m} &= \mathrm{E}\left\{\bar{\mathbf{y}}_m[p]\bar{\mathbf{y}}_m^H[p]\right\} \\ &= \mathbf{A}_m(l_r,\boldsymbol{\theta}_m)\mathbf{R}_{\mathbf{u}_m}\mathbf{A}_m^H(l_r\boldsymbol{\theta}_m) + \sigma_m^2\overline{\mathbf{T}}_m \ , \end{aligned} \tag{16}$$

where $\mathrm{E}\{\cdot\}$ is the expectation operator, and $\mathbf{R}_{\mathbf{u}_m} = \mathrm{E}\left\{\mathbf{u}_m[p]\mathbf{u}_m^H[p]\right\}$ is the covariance matrix of the equivalent received signals. Under the white Gaussian noise assumption where $\sigma_m^2[l_j] = \sigma_m^2$, $\forall j = 0,1,\ldots,J-1$, we have $\sigma_m^2\overline{\mathbf{T}}_m = \sum_{j=0}^{J-1}\sigma_m^2[l_j]\mathbf{T}_m[l_j]\mathbf{T}_m^H[l_j] = \sigma_m^2\sum_{j=0}^{J-1}\mathbf{T}_m[l_j]\mathbf{T}_m^H[l_j]$.

Defining $\mathbf{P}_m = \mathbf{R}_{\mathbf{u}_m}\mathbf{A}_m^H(l_r,\boldsymbol{\theta}_m)$, we have

$$\mathbf{R}_{\bar{\mathbf{y}}_m} = \mathbf{A}_m(l_r,\boldsymbol{\theta}_m)\mathbf{P}_m + \sigma_m^2\overline{\mathbf{T}}_m \ . \tag{17}$$

Under the CS framework, a search grid of K_g ($K_g \gg K$) potential incident angles $\theta_{g,0},\theta_{g,1},\ldots,\theta_{g,K_g-1}$ is first generated, and an overcomplete representation of $\mathbf{A}_m(l_r,\boldsymbol{\theta_g})$ is then constructed, given by

$$\mathbf{A}_m(l_r,\boldsymbol{\theta_g}) = \left[\mathbf{a}_m(l_r,\theta_{g,0}),\ldots,\mathbf{a}_m(l_r,\theta_{g,K_g-1})\right] \ . \tag{18}$$

By applying the group sparsity concept, the ℓ_1-SRACV [25] method is formulated as

$$\begin{aligned} \min_{\mathbf{P}_{\mathbf{g},m},\sigma_m^2} \quad & \left\|\mathbf{p}_{\mathbf{g},m}^{\circ}\right\|_1 \\ \text{subject to} \quad & \left\|\mathbf{R}_{\bar{\mathbf{y}}_m} - \mathbf{A}_m(l_r,\boldsymbol{\theta}_{\boldsymbol{g}})\mathbf{P}_{\mathbf{g},m} - \sigma_m^2\overline{\mathbf{T}}_m\right\|_F \le \varepsilon \ , \end{aligned} \tag{19}$$

where $\|\cdot\|_1$ is the ℓ_1 norm, and $\mathbf{P}_{\mathbf{g},m}$ is a constructed $K_g \times L_m$ matrix with $\mathbf{p}_m^{k_g}$ being its k_g-th row vector, representing the potential signals at the corresponding incident angle. ε is the allowable error bound, and $\mathbf{p}_{\mathbf{g},m}^{\circ} = [\mathbf{p}_{\mathbf{g},m}^T, \sigma_m^2]^T$ is a $(K_g + 1) \times 1$ column vector with

$$\mathbf{p}_{\mathbf{g},m} = \left[\left\|\mathbf{p}_m^0\right\|_2, \left\|\mathbf{p}_m^1\right\|_2, \ldots, \left\|\mathbf{p}_m^{K_g-1}\right\|_2\right]^T , \tag{20}$$

where $\|\cdot\|_2$ is the ℓ_2 norm.

The elements in $\mathbf{p}_{\mathbf{g},m}$ are the corresponding DOA estimation results over the K_g search grids, while σ_m^2 is also considered as an unknown variable to be estimated. Denote the obtained DOA results from solving (19) as $\tilde{\boldsymbol{\theta}}_m$, and they can be converted to the predefined Cartesian coordinate system by $\tilde{\boldsymbol{\phi}}_m = \tilde{\boldsymbol{\theta}}_m - \varphi_m$.

Remark 2: It is noted that although the number of elements to be estimated in the optimization problem (19) is increased compared with the ℓ_1-SVD method [24], the prior knowledge of the rank of $\mathbf{R}_{\mathbf{s}_m}$ is not required and better estimation results can be obtained especially for low input signal to noise ratios (SNRs) due to involvement of the noise power estimation in the optimization.

D. Group Sparsity Based DOA Estimation across All Observation Platforms

Due to different propagation delays, rotation angles, and propagation coefficients among sub-arrays, it is difficult to merge those signal models at all sub-arrays together through traditional methods. However, all the array signal models share the same spatial support for far-field sources based on the predefined Cartesian coordinate system, but with different angle offsets equal to their rotation angles. To exploit the information acquired by all the sub-arrays jointly, we force a common sparsity of the DOAs across all the distributed platforms, and the group sparsity concept can be employed again for DOA estimation.

Denote $\boldsymbol{\phi}_{\boldsymbol{g}} = \left[\phi_{g,0}, \phi_{g,1}, \ldots, \phi_{g,K_g-1}\right]^T$ as a search grid of K_g potential incident angles in the Cartesian coordinate system. Then, the equivalent search grid based on each rotated sub-array is $\boldsymbol{\theta}_{\boldsymbol{g},m} = \boldsymbol{\phi}_{\boldsymbol{g}} + \varphi_m$, $m = 1, 2, \ldots, M$. As a result, we can rewrite the signal model from the sparse signal reconstruction perspective as

$$\mathbf{R}_{\bar{\mathbf{y}}_m} = \mathbf{A}_m(l_r,\boldsymbol{\theta}_{\boldsymbol{g},m})\mathbf{P}_{\mathbf{g},m} + \sigma_m^2\overline{\mathbf{T}}_m \ , \tag{21}$$

where the search grid employed in $\mathbf{A}_m(l_r,\boldsymbol{\theta}_{\boldsymbol{g},m})$ and $\mathbf{P}_{\mathbf{g},m}$ is replaced by $\boldsymbol{\theta}_{\boldsymbol{g},m}$.

For far-field sources where the incident angles of the same source on different sub-arrays are considered to be the same, we can estimate the DOAs of the sources jointly by extending the group sparsity concept across all the sub-arrays due to the same spatial support, although the array models may have varying values in the matrix $\mathbf{P}_{\mathbf{g},m}$, $m = 1, 2, \ldots, M$ to be estimated, and different steering vectors caused by the rotation angles as well as the possible different sub-array sensor numbers.

TABLE I
PROCEDURE OF THE PROPOSED GS-SRACV METHOD

Step 1)	Apply the focusing algorithm in (11) to form a combined signal model (12) with reduced dimension. For the selection strategy of $\boldsymbol{\theta}_{\boldsymbol{F}}$, please refer to *Remark 5*, and similar strategy given in Table II can be employed with associated changes.
Step 2)	Based on each $\mathbf{R}_{\bar{\mathbf{y}}_m}$ with the size of $L_m \times L_m$, the DOAs of the far-field sources can be estimated by applying the proposed GS-SRACV method in (25).
Output	The first K_g elements of the column vector $\mathbf{u}_{\mathbf{g}}^{\circ}$ are the corresponding DOA estimation results over the K_g search grids in $\boldsymbol{\phi}_{\boldsymbol{g}}$.

To facilitate the formulation, we vectorize the covariance matrix of the m-th sub-array as

$$\mathbf{z}_m = \mathrm{vec}\left\{\mathbf{R}_{\bar{\mathbf{y}}_m}\right\} = \mathrm{vec}\left\{\mathbf{A}_m(l_r,\boldsymbol{\theta}_m)\mathbf{P}_m + \sigma_m^2\overline{\mathbf{T}}_m\right\} . \tag{22}$$

Under the CS framework, we denote the column vector $\mathbf{b}_{\mathbf{g},m}$ as

$$\mathbf{b}_{\mathbf{g},m} = \mathrm{vec}\left\{\mathbf{A}_m(l_r,\boldsymbol{\theta}_{\boldsymbol{g},m})\mathbf{P}_{\mathbf{g},m} + \sigma_m^2\overline{\mathbf{T}}_m\right\} . \tag{23}$$

Then, we construct a $\sum_{m=1}^{M} L_m^2 \times 1$ column vector $\mathbf{z}$ and a $K_g \times L$ matrix $\mathbf{U}_{\mathbf{g}}$ by

$$\begin{aligned} \mathbf{z} &= \left[\mathbf{z}_1^T, \mathbf{z}_2^T, \ldots, \mathbf{z}_M^T\right]^T , \\ \mathbf{U}_{\mathbf{g}} &= \left[\mathbf{P}_{\mathbf{g},1}, \mathbf{P}_{\mathbf{g},2}, \ldots, \mathbf{P}_{\mathbf{g},M}\right] , \end{aligned} \tag{24}$$

with $L = \sum_{m=1}^{M} L_m$ and row vector $\mathbf{u}_{\mathbf{g}}^{k_g}$, $0 \le k_g \le K_g$, as the k_g-th row of the matrix $\mathbf{U}_{\mathbf{g}}$.

Finally, the DOA estimation method employing the group sparsity concept based on ℓ_1-SRACV (referred to as GS-SRACV) across all distributed platforms is formulated as follows

$$\min_{\mathbf{U}_{\mathbf{g}},\sigma_m^2} \quad \left\|\mathbf{u}_{\mathbf{g}}^{\circ}\right\|_1 \quad \text{subject to} \quad \left\|\mathbf{z} - \mathbf{b}_{\mathbf{g}}\right\|_2 \le \varepsilon \ , \tag{25}$$

where the column vector $\mathbf{u}_{\mathbf{g}}^{\circ}$ is formed by applying ℓ_2 norm to each row vector $\mathbf{u}_{\mathbf{g}}^{k_g}$ and the noise terms across all the sub-arrays, expressed as

$$\mathbf{u}_{\mathbf{g}}^{\circ} = \left[\left\|\mathbf{u}_{\mathbf{g}}^0\right\|_2, \left\|\mathbf{u}_{\mathbf{g}}^1\right\|_2, \ldots, \left\|\mathbf{u}_{\mathbf{g}}^{K_g-1}\right\|_2, \sigma_{\bar{n}}^2\right]^T , \tag{26}$$

with

$$\sigma_{\bar{n}}^2 = \left\| \left[\sigma_1^2, \sigma_2^2, \ldots, \sigma_M^2\right] \right\|_2 \tag{27}$$

being the ℓ_2 norm of all the noises at different sub-arrays, and $\mathbf{b}_{\mathbf{g}} = \left[\mathbf{b}_{\mathbf{g},1}^T, \mathbf{b}_{\mathbf{g},2}^T, \ldots, \mathbf{b}_{\mathbf{g},M}^T\right]^T$.

Note that all noise powers are considered as unknown variables to be estimated. The first K_g elements of the column vector $\mathbf{u}_{\mathbf{g}}^{\circ}$ are the corresponding DOA estimation results over the K_g search grids in $\boldsymbol{\phi}_{\boldsymbol{g}}$. The procedure of the proposed GS-SRACV method is summarized in Table I.

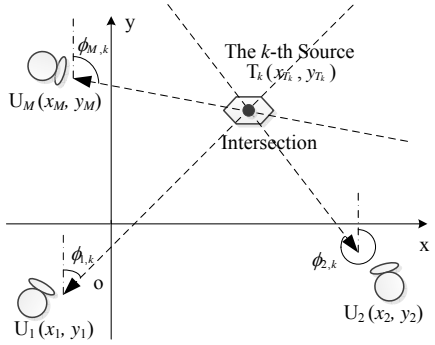

Fig. 4. A typical localization geometry for near-field sources.

IV. Localization for Near-Field Sources

For near-field sources, the incident angles of the same source for different sub-arrays are not the same and may be quite different, i.e., $\phi_{m_1,k} \neq \phi_{m_2,k}$ for $m_1 \neq m_2$. However, all the sources are still assumed to be relatively far-field compared to each sub-array aperture. As a result, the DOA estimation method for far-field sources can not be applied directly due to their different DOA support. In this section, the group sparsity concept is further extended to the two-dimensional (2-D) case to solve the near-field source localization problem.

A. Group Sparsity Based 2-D Localization for Near-Field Sources

Ideally in the noiseless case, the source position can be uniquely determined by the intersection of the lines-of-sight associated with the AOAs from two or more subarrays. In the presence of noise, the triangulation or fixing methods are required to ensure the unique localization [4], [12] without ambiguous solutions. A typical localization geometry for near-field sources is shown in Fig. 4, where for a given source position $T_k(x_{T_k}, y_{T_k})$, there is a unique incident angle $\theta_{m,k}$ for each sub-array. We can localize the sources by forcing a common sparse structure in the predefined Cartesian coordinate system across all sub-arrays, and an effective group sparsity based 2-D localization method (GS-Localization) is proposed through jointly exploiting the information acquired by all sub-arrays.

Without loss of generality, the area of interest in the Cartesian coordinate system is assumed to be a square shape, and it is divided into K_xK_y grids, where K_x is the number of grids along the x-axis, while K_y is the number along the y-axis. Denote $G(x_{k_x}, y_{k_y})$, $k_x = 0, 1, \ldots, K_x - 1$ and $k_y = 0, 1, \ldots, K_y - 1$, as the position of the (k_x, k_y)-th search grid. Then, we generate its corresponding incident angle $\theta_{g,m}(k_x, k_y)$ based on the m-th sub-array, expressed as

$$\theta_{g,m}(k_x, k_y) = \arctan 2(\Delta x_{m,k_x}, \Delta y_{m,k_y}) + \varphi_m \ , \quad (28)$$

with

$$\Delta x_{m,k_x} = x_{k_x} - x_m \ , \ \ \Delta y_{m,k_y} = y_{k_y} - y_m \ . \quad (29)$$

We construct a $K_xK_y \times 1$ column vector consisting of all potential incident angles by stacking $\theta_g(k_x, k_y)$, $k_x = 0, 1, \ldots, K_x - 1$ and $k_y = 0, 1, \ldots, K_y - 1$, given by

$$\begin{aligned}\tilde{\boldsymbol{\theta}}_{\boldsymbol{g},m} = \big[&\theta_{g,m}(0,0), \theta_{g,m}(0,1), \ldots, \theta_{g,m}(0, K_y - 1), \\ &\theta_{g,m}(1,0), \theta_{g,m}(1,1), \ldots, \theta_{g,m}(1, K_y - 1), \\ &\ldots\ldots \\ &\theta_{g,m}(K_x - 1, 0), \ldots, \theta_{g,m}(K_x - 1, K_y - 1)\big]^T \ .\end{aligned} \quad (30)$$

Then for each sub-array, the focusing algorithm is still applied first to deal with the wideband signals as presented in Sec. III-A, and the array model after focusing under the CS framework can be represented as

$$\mathbf{R}_{\bar{\mathbf{y}}_m} = \mathbf{A}_m(l_r, \tilde{\boldsymbol{\theta}}_{\boldsymbol{g},m})\tilde{\mathbf{P}}_{\mathbf{g},m} + \sigma_m^2 \overline{\mathbf{T}}_m \ , \quad (31)$$

where each row vector in the $K_xK_y \times L_m$ matrix $\tilde{\mathbf{P}}_{\mathbf{g},m}$ is the signals corresponding to the grid at the same row in $\tilde{\boldsymbol{\theta}}_{\boldsymbol{g},m}$.

The 2-D grids in the predefined Cartesian coordinate system is converted to the incident angle domain, and sparsity can be forced in the area of interest for source localization due to the uniqueness of the incident angle group $\theta_{g,m}(k_x, k_y)$, $m = 1, 2, \ldots, M$ for each grid.

Similarly, vectorizing the signal covariance matrix of the m-th sub-array yields

$$\tilde{\mathbf{z}}_m = \mathrm{vec}\left\{\mathbf{R}_{\bar{\mathbf{y}}_m}\right\} = \mathrm{vec}\left\{\mathbf{A}_m(l_r, \boldsymbol{\theta}_m)\mathbf{P}_m + \sigma_m^2 \overline{\mathbf{T}}_m\right\} \ . \quad (32)$$

Under the CS framework, denote

$$\tilde{\mathbf{b}}_{\mathbf{g},m} = \mathrm{vec}\left\{\mathbf{A}_m(l_r, \tilde{\boldsymbol{\theta}}_{\boldsymbol{g},m})\tilde{\mathbf{P}}_{\mathbf{g},m} + \sigma_m^2 \overline{\mathbf{T}}_m\right\} \ , \quad (33)$$

and then a $K_xK_y \times L$ matrix $\tilde{\mathbf{U}}_{\mathbf{g}}$ is generated by

$$\tilde{\mathbf{U}}_{\mathbf{g}} = \left[\tilde{\mathbf{P}}_{\mathbf{g},1}, \tilde{\mathbf{P}}_{\mathbf{g},2}, \ldots, \tilde{\mathbf{P}}_{\mathbf{g},M}\right] \ , \quad (34)$$

with row vector $\tilde{\mathbf{u}}_{\mathbf{g}}^{k_g}$, $0 \leq k_g \leq K_xK_y - 1$, as the k_g-th row of the matrix $\tilde{\mathbf{U}}_{\mathbf{g}}$.

Based on the generated grids, the entries in each row vector $\tilde{\mathbf{u}}_{\mathbf{g}}^{k_g}$ are associated with the same location $G(x_{k_x}, y_{k_y})$, where $k_g = k_x \cdot K_x + k_y$, and therefore share the same two-dimensional support. By applying ℓ_2 norm to $\mathbf{u}_{\mathbf{g}}^{k_g}$ and the noise terms across all the sub-arrays, we have

$$\tilde{\mathbf{u}}_{\mathbf{g}}^{\circ} = \left[\left\|\tilde{\mathbf{u}}_{\mathbf{g}}^{0}\right\|_2, \left\|\tilde{\mathbf{u}}_{\mathbf{g}}^{1}\right\|_2, \ldots, \left\|\tilde{\mathbf{u}}_{\mathbf{g}}^{K_xK_y-1}\right\|_2, \tilde{\sigma}_{\bar{n}}^2\right]^T \ , \quad (35)$$

with

$$\tilde{\sigma}_{\bar{n}}^2 = \left\| \left[\sigma_1^2, \sigma_2^2, \ldots, \sigma_M^2\right] \right\|_2 \ . \quad (36)$$

Considering all the noise terms and the matrix $\tilde{\mathbf{U}}_{\mathbf{g}}$ as unknown variables to be estimated, the group sparsity based 2-D localization problem (GS-Localization) can be formulated as

$$\min_{\tilde{\mathbf{U}}_{\mathbf{g}}, \sigma_m^2} \ \ \left\|\tilde{\mathbf{u}}_{\mathbf{g}}^{\circ}\right\|_1 \ \ \text{subject to} \ \ \left\|\tilde{\mathbf{z}} - \tilde{\mathbf{b}}_{\mathbf{g}}\right\|_2 \leq \varepsilon \ , \quad (37)$$

where $\tilde{\mathbf{z}}$ and $\tilde{\mathbf{b}}_{\mathbf{g}}$ are both $K_xK_yL \times 1$ column vectors given by

$$\begin{aligned}\tilde{\mathbf{z}} &= \left[\tilde{\mathbf{z}}_1^T, \tilde{\mathbf{z}}_2^T, \ldots, \tilde{\mathbf{z}}_M^T\right]^T \ , \\ \tilde{\mathbf{b}}_{\mathbf{g}} &= \left[\tilde{\mathbf{b}}_{\mathbf{g},1}^T, \tilde{\mathbf{b}}_{\mathbf{g},2}^T, \ldots, \tilde{\mathbf{b}}_{\mathbf{g},M}^T\right]^T \ .\end{aligned} \quad (38)$$

The first K_xK_y elements of the column vector $\tilde{\mathbf{u}}_{\mathbf{g}}^{\circ}$ are the corresponding localization results over the K_xK_y search grids, which are finally translated to the source positions in the Cartesian coordinate system.

Remark 3: In the proposed solution GS-SRACV (25) for the far-field sources and the GS-Localization (37) for near-field sources, the information collected by the entire distributed array network is utilized directly in solving the optimization problems. Compared with the MLE where only the separate DOA estimation results obtained by sub-arrays are involved in the RMSE minimization problem, improved performance and robustness can be achieved by our proposed solutions.

Remark 4: It is worth nothing that only the covariance matrix with the size of $L_m \times L_m$ for each sub-array instead of all the data samples is required for centralized processing, and therefore the additional data exchange workload is rather limited compared with those AOA-based fusion methods.

B. Grid Refining Strategy for Complexity Reduction

The GS-Localization method finds the common sparsity in the 2-D Cartesian coordinate system, and the computational complexity would be extremely high if a large number of grids are involved for a more accurate result. Therefore, instead of employing a universally fine search grid, we extend the idea of adaptively refining the search grid in DOA estimation to the 2-D case for complexity reduction without sacrificing the performance.

Denote α_q as the step size in the q-th step, $\tilde{\boldsymbol{\theta}}_{\boldsymbol{g},m}^{q}$ is the vector of updated incident potential angles associated with the refined search grid in the q-th step, and $\tilde{T}_k^q(\tilde{x}_{T_k}^q, \tilde{y}_{T_k}^q)$ is the estimated position of the k-th source in the q-th step. For a Q-Step grid refining strategy, we first generate a search grid with a large step size α_1 in the entire area of interest, and coarse position estimates of the sources can be found by applying the proposed GS-Localization method in (37), expressed as $\tilde{T}_k^1(\tilde{x}_{T_k}^1, \tilde{y}_{T_k}^1)$. Next we focus on the areas around the positions estimated, and an updated search grid is generated in $\tilde{x}_{T_k}^1 - \alpha_1 \le x \le \tilde{x}_{T_k}^1 + \alpha_1$ and $\tilde{y}_{T_k}^1 - \alpha_1 \le y \le \tilde{y}_{T_k}^1 + \alpha_1$ with a smaller step size $\alpha_2 = \frac{\alpha_1}{\gamma}$. Then the $\tilde{\tilde{\boldsymbol{\theta}}}_{\boldsymbol{g},m}^{2}$ corresponding to the new search grid is obtained, and the GS-Localization method is applied again with the refined search grid to obtain the localization results $\tilde{T}_k^2(\tilde{x}_{T_k}^2, \tilde{y}_{T_k}^2)$. The aforementioned step is repeated Q times to ensure the grid is fine enough, where at the q-th step, the search grid refined in the updated areas

$$\begin{aligned} \tilde{x}_{T_k}^{q-1} - \alpha_{q-1} \le x \le \tilde{x}_{T_k}^{q-1} + \alpha_{q-1} \ , \\ \tilde{y}_{T_k}^{q-1} - \alpha_{q-1} \le y \le \tilde{y}_{T_k}^{q-1} + \alpha_{q-1} \ , \end{aligned} \tag{39}$$

is employed, where $k = 1, 2, \ldots, K$ and $\alpha_q = \frac{\alpha_{q-1}}{\gamma}$.

The procedure of the grid refining strategy is summarized in Table II.

Remark 5: Note that for the narrowband case with $J = 1$, the proposed solutions for both far-field and near-field sources in Sec. III and Sec. IV are still effective without the focusing process. As well-known, the performance of focusing is sensitive to the initial DOAs $\boldsymbol{\theta}_{\boldsymbol{F}}$, which can be updated iteratively to obtain a good performance [46], [66], or we can simply use the refined grids in each step as the focusing angles [45].

TABLE II
PROCEDURE OF THE PROPOSED GS-LOCALIZATION METHOD WITH GRID REFINING STRATEGY

Step 1)	Initialize $q = 1$ and generate a coarse search grid in the entire area of interest with a large step size α_1.
Step 2)	Apply the focusing algorithm in (11) to form a combined signal model (12) with reduced dimension. For the selection strategy of $\boldsymbol{\theta}_{\boldsymbol{F}}$, please refer to *Remark 5*.
Step 3)	Estimate the source locations by applying the proposed GS-Localization method in (37) with the results given as $\tilde{T}_k^q(\tilde{x}_{T_k}^q, \tilde{y}_{T_k}^q)$.
Step 4)	Set $q = q + 1$, an updated search grid is generated in the refined areas in (39) with a smaller step size $\alpha_q = \frac{\alpha_{q-1}}{\gamma}$.
Step 5)	Re-focusing if necessary (See *Remark 5* and also [45], [46], [66]).
Step 6)	Based on the $\tilde{\boldsymbol{\theta}}_{\boldsymbol{g},m}^{q}$ associated with the newly updated search grid, solve the localization problem by applying the GS-Localization method to obtain the source locations $\tilde{T}_k^q(\tilde{x}_{T_k}^q, \tilde{y}_{T_k}^q)$.
Step 7)	Repeat steps 4) to 6) until $q = Q$, and $\tilde{T}_k(\tilde{x}_{T_k}^Q, \tilde{y}_{T_k}^Q)$, $k = 1, 2, \ldots, K$, are the final estimation results of the source locations.
Output	$\tilde{T}_k(\tilde{x}_{T_k}^Q, \tilde{y}_{T_k}^Q)$, $k = 1, 2, \ldots, K$, are the final estimation results of the source locations.

V. CRAMÉR-RAO BOUNDS

For far-field sources, the CRB in the wideband scenario based on subarray systems or distributed sensor array networks has not been studied yet. For near-field sources, existing CRB is derived from corrupted AOA/DOA measurements instead of the original data samples. Therefore, we derive the CRBs for far-field sources and near-field sources in this section.

A. CRB for the Far-Field Case

Based on the stochastic model, the sources and noises are assumed to be zero-mean Gaussian processes, and the noises are spatially uncorrelated. For each sub-array, the time duration of each data group with L samples is usually much larger than the correlation time of the source signals and noise, and thus P non-overlapping groups yield P independent and identically distributed (i.i.d.) frequency snapshots [69], [70].

Denote $w(\mathbf{X}_m[l_j, p]; \boldsymbol{\alpha})$ as the probability density function (p.d.f.) of $\mathbf{X}_m[l_j, p]$, which depends on the vector $\boldsymbol{\alpha}$ holding real-valued unknown parameters. Then, the joint p.d.f. of all frequency domain samples can be expressed as

$$\bar{w} = \prod_{m=1}^{M} \prod_{j=1}^{J} \prod_{p=1}^{P} w(\mathbf{X}_m[l_j, p]; \boldsymbol{\alpha}) \ . \tag{40}$$

The Fisher Information Matrix (FIM) for $\mathbf{X}_m[l_j, p]$ is defined as [71]

$$\mathbf{F}_m[l_j, p] \triangleq -E\left[\frac{\partial^2 \ln w(\mathbf{X}_m[l_j, p]; \boldsymbol{\alpha})}{\partial \boldsymbol{\alpha} \, \partial \boldsymbol{\alpha}^T}\right]. \tag{41}$$

Since the P frequency snapshots are i.i.d., we have $\{\mathbf{F}_m[l_j, p]\}_{p=1}^{P} = \mathbf{F}_m[l_j]$. Combining (40) and (41), the FIM obtained from the distributed sensor array network within the frequency bins of interest is expressed as

$$\bar{\mathbf{F}} = P \sum\nolimits_{m=1}^{M} \sum\nolimits_{j=1}^{J} \mathbf{F}_m[l_j] \ . \tag{42}$$

Denote the covariance matrix of $\mathbf{X}_m[l_j,p]$ as $\mathbf{R}_{\mathbf{X}_m}[l_j]$. Then, $\mathbf{F}_m[l_j]$ is given by [72]

$$\begin{aligned}\mathbf{F}_m[l_j] &= \mathrm{tr}\left(\mathbf{R}_{\mathbf{X}_m}^{-1}[l_j]\frac{\partial \mathbf{R}_{\mathbf{X}_m}[l_j]}{\partial \boldsymbol{\alpha}^T}\mathbf{R}_{\mathbf{X}_m}^{-1}[l_j]\frac{\partial \mathbf{R}_{\mathbf{X}_m}[l_j]}{\partial \boldsymbol{\alpha}^T}\right)\\ &= \left(\mathbf{W}_m[l_j]\frac{\partial \mathbf{r}_m[l_j]}{\partial \boldsymbol{\alpha}^T}\right)^H\left(\mathbf{W}_m[l_j]\frac{\partial \mathbf{r}_m[l_j]}{\partial \boldsymbol{\alpha}^T}\right),\end{aligned} \tag{43}$$

where

$$\begin{aligned}\mathbf{W}_m[l_j] &= (\mathbf{R}_{\mathbf{X}_m}^T[l_j]\otimes \mathbf{R}_{\mathbf{X}_m}[l_j])^{-\frac{1}{2}},\\ \mathbf{r}_m[l_j] &= \mathrm{vec}\{\mathbf{R}_{\mathbf{X}_m}[l_j]\},\end{aligned} \tag{44}$$

with $\otimes$ denoting the Kronecker product.

In the far-field case, $\boldsymbol{\alpha}$ is given by

$$\boldsymbol{\alpha} = \boldsymbol{\alpha}_{\text{far}} = [\tilde{\boldsymbol{\phi}}^T, \tilde{\mathbf{q}}^T, \boldsymbol{\sigma}^T]^T, \tag{45}$$

where

$$\begin{aligned}\tilde{\boldsymbol{\phi}} &= [\phi_1,\ldots,\phi_K]^T, & \tilde{\mathbf{q}} &= [\bar{\mathbf{q}}_1^T,\ldots,\bar{\mathbf{q}}_M^T]^T,\\ \bar{\mathbf{q}}_m &= [\mathbf{q}_m^T[l_1],\ldots,\mathbf{q}_m^T[l_J]]^T, & \boldsymbol{\sigma} &= [\sigma_1^2,\ldots,\sigma_M^2]^T,\end{aligned} \tag{46}$$

and $\mathbf{q}_m[l_j]$ contains the real and imaginary parts of the upper triangular elements in $\mathbf{R}_{\mathbf{S}_m}[l_j]$, which is the covariance matrix of $\mathbf{S}_m[l_j,p]$.

To calculate the derivatives of $\mathbf{r}_m[l_j]$ w.r.t. $\boldsymbol{\alpha}$, we rewrite $\mathbf{r}_m[l_j]$ as

$$\mathbf{r}_m[l_j] = \mathbf{C}_m[l_j]\boldsymbol{\Psi}\mathbf{q}_m[l_j] + \sigma_m^2\mathbf{i}_m, \tag{47}$$

where

$$\begin{aligned}\mathbf{C}_m[l_j] &= \mathbf{A}_m^*(l_j,\boldsymbol{\theta}_m)\otimes\mathbf{A}_m(l_j,\boldsymbol{\theta}_m),\\ \mathbf{i}_m &= \mathrm{vec}\{\mathbf{I}_{L_m}\},\end{aligned} \tag{48}$$

and $\boldsymbol{\Psi}$ is a $K^2\times K^2$ nonsingular matrix satisfying [72]

$$\mathrm{vec}\{\mathbf{R}_{\mathbf{S}_m}[l_j]\} = \boldsymbol{\Psi}\mathbf{q}_m[l_j]. \tag{49}$$

For the far-field case, the first block of $\frac{\partial \mathbf{r}_m[l_j]}{\partial \boldsymbol{\alpha}^T}$ is

$$\frac{\partial \mathbf{r}_m[l_j]}{\partial \tilde{\boldsymbol{\phi}}^T} = \dot{\mathbf{C}}_m[l_j], \tag{50}$$

where

$$\begin{aligned}\dot{\mathbf{C}}_m[l_j] &= [\mathbf{A}_m^*(l_j,\boldsymbol{\theta}_m)\otimes\dot{\mathbf{A}}_m(l_j,\boldsymbol{\theta}_m)]\mathbf{E}_m[l_j]\\ &\quad+[\dot{\mathbf{A}}_m^*(l_j,\boldsymbol{\theta}_m)\otimes\mathbf{A}_m(l_j,\boldsymbol{\theta}_m)]\mathbf{E}'_m[l_j],\\ \mathbf{E}_m[l_j] &= \left[\mathrm{vec}\{\mathbf{f}_1\mathbf{f}_1^T\mathbf{R}_{\mathbf{S}_m}[l_j]\},\cdots,\mathrm{vec}\{\mathbf{f}_K\mathbf{f}_K^T\mathbf{R}_{\mathbf{S}_m}[l_j]\}\right],\\ \mathbf{E}'_m[l_j] &= \left[\mathrm{vec}\{\mathbf{R}_{\mathbf{S}_m}[l_j]\mathbf{f}_1\mathbf{f}_1^T\},\cdots,\mathrm{vec}\{\mathbf{R}_{\mathbf{S}_m}[l_j]\mathbf{f}_K\mathbf{f}_K^T\}\right],\\ \dot{\mathbf{A}}_m(l_j,\boldsymbol{\theta}_m) &= [\dot{\mathbf{a}}_m(l_j,\theta_{m,1}),\cdots,\dot{\mathbf{a}}_m(l_j,\theta_{m,K})],\\ \dot{\mathbf{a}}_m(l_j,\theta_{m,k}) &= \frac{\partial \mathbf{a}_m(l_j,\theta_{m,k})}{\partial\phi_k},\end{aligned} \tag{51}$$

with $\mathbf{f}_k$ being a $K\times 1$ vector containing a one at the k-th position and zeros elsewhere. The v-th ($v=0,1,\ldots,L_m$) element of $\dot{\mathbf{a}}_m(l_j,\theta_{m,k})$ is given by

$$[\dot{\mathbf{a}}_m(l_j,\theta_{m,k})]_v = -j\frac{2\pi\hbar_v^m d}{\lambda_f}\cos(\theta_{m,k})e^{-j\frac{2\pi\hbar_v^m d}{\lambda_f}\sin(\theta_{m,k})}.$$

The second block can be expressed as

$$\frac{\partial \mathbf{r}_m[l_j]}{\partial \tilde{\mathbf{q}}^T} = \bar{\mathbf{e}}_{(m-1)J+l_j}\otimes\{\mathbf{C}_m[l_j]\boldsymbol{\Psi}\}, \tag{52}$$

where $\bar{\mathbf{e}}_{(m-1)J+l_j}$ is a $1\times MJ$ vector containing a one at the $[(m-1)J+l_j]$-th position and zeros elsewhere.

The third block is given by

$$\frac{\partial \mathbf{r}_m[l_j]}{\partial \boldsymbol{\sigma}^T} = \mathbf{e}_m\otimes\mathbf{i}_m, \tag{53}$$

with $\mathbf{e}_m$ denoting a $1\times M$ vector containing a one at the m-th position and zeros elsewhere.

By substituting (50), (52), (53) into (43), we can obtain the FIM in (42) for far-field sources, and the CRB is given by

$$\mathbf{B} = \bar{\mathbf{F}}^{-1}, \tag{54}$$

where we are only interested in the first principal $K\times K$ sub-matrix in $\mathbf{B}$ corresponding to DOAs [70].

Although (54) can be used to calculate the CRB, it is rather complicated and only the DOA-related block of the CRB matrix is of interest.

To derive a closed-form CRB for the DOA part, we first introduce the following notations.

$$\begin{aligned}&\bar{\mathbf{W}}_m = \mathrm{blkdiag}\{\mathbf{W}_m[l_1],\ldots,\mathbf{W}_m[l_J]\},\\ &\bar{\dot{\mathbf{C}}}_m = \left[\dot{\mathbf{C}}_m^T[l_1],\ldots,\dot{\mathbf{C}}_m^T[l_J]\right]^T, \quad \bar{\mathbf{i}}_m = \mathbf{1}_J\otimes\mathbf{i}_m,\\ &\bar{\mathbf{C}}_m = \mathrm{blkdiag}\{\mathbf{C}_m[l_1]\boldsymbol{\Psi},\ldots,\mathbf{C}_m[l_J]\boldsymbol{\Psi}\},\end{aligned} \tag{55}$$

where $\mathrm{blkdiag}\{\cdot\}$ is the block diagonalization operation, and $\mathbf{1}_J$ is a $J\times 1$ all-one vector.

We combine all the sub-array components as follows.

$$\begin{aligned}&\tilde{\mathbf{W}} = \mathrm{blkdiag}\{\bar{\mathbf{W}}_1,\ldots,\bar{\mathbf{W}}_M\}, \quad \tilde{\dot{\mathbf{C}}} = [\bar{\dot{\mathbf{C}}}_1^T,\ldots,\bar{\dot{\mathbf{C}}}_M^T]^T,\\ &\tilde{\mathbf{C}} = \mathrm{blkdiag}\{\bar{\mathbf{C}}_1,\ldots,\bar{\mathbf{C}}_M\}, \quad \tilde{\mathbf{i}} = \mathrm{blkdiag}\{\bar{\mathbf{i}}_1,\ldots,\bar{\mathbf{i}}_M\}.\end{aligned} \tag{56}$$

Then, $\bar{\mathbf{F}}$ can be rewritten as

$$\bar{\mathbf{F}} = P\begin{bmatrix}\mathbf{G}^H\\ \boldsymbol{\Delta}^H\end{bmatrix}[\mathbf{G},\boldsymbol{\Delta}], \tag{57}$$

where

$$\mathbf{G} = \tilde{\mathbf{W}}\tilde{\dot{\mathbf{C}}}, \quad \boldsymbol{\Delta} = \tilde{\mathbf{W}}[\tilde{\mathbf{C}},\tilde{\mathbf{i}}]. \tag{58}$$

Using the standard result on the inversion of a partitioned matrix [73], we can obtain the closed-form CRB expression for DOAs alone in the far-field case:

$$\mathbf{B}_{\boldsymbol{\theta}} = (P\mathbf{G}^H\boldsymbol{\Pi}_{\boldsymbol{\Delta}}^{\perp}\mathbf{G})^{-1}, \tag{59}$$

where $\boldsymbol{\Pi}_{\boldsymbol{\Delta}}^{\perp} = \mathbf{I}_{J\sum_{m=1}^M L_m^2} - \boldsymbol{\Delta}(\boldsymbol{\Delta}^H\boldsymbol{\Delta})^{-1}\boldsymbol{\Delta}^H$ is the orthogonal projector onto the null space of $\boldsymbol{\Delta}^H$.

B. CRB for the Near-Field Case

In the near-field case, the positions of the sources are represented by $\mathbf{T}_k = (x_{T_k}, y_{T_k})$, $k=1,\cdots,K$. Thus, the unknown parameter vector is

$$\boldsymbol{\alpha} = \boldsymbol{\alpha}_{\text{near}} = [\bar{\mathbf{T}}_x^T, \bar{\mathbf{T}}_y^T, \tilde{\mathbf{q}}^T, \boldsymbol{\sigma}^T]^T, \tag{60}$$

where

$$\bar{\mathbf{T}}_x = [x_{T_1},\cdots,x_{T_K}]^T, \quad \bar{\mathbf{T}}_y = [y_{T_1},\cdots,y_{T_K}]^T. \tag{61}$$

Calculating the derivatives of the v-th element of $\mathbf{a}_m(l_j,\theta_{m,k})$ w.r.t. x_{T_k} and y_{T_k} respectively yields

$$\begin{aligned}&\left[\frac{\partial \mathbf{a}_m(l_j,\theta_{m,k})}{\partial x_{T_k}}\right]_v\\ &= -j\frac{2\pi\hbar_v^m d}{\lambda_f}\cos(\theta_{m,k})\frac{\Delta y_{m,k}}{\Delta x_{m,k}^2+\Delta y_{m,k}^2}e^{-j\frac{2\pi\hbar_v^m d}{\lambda_f}\sin(\theta_{m,k})},\end{aligned} \tag{62}$$

$$\left[\frac{\partial \mathbf{a}_m(l_j,\theta_{m,k})}{\partial y_{T_k}}\right]_v = j\frac{2\pi\hbar_v^m d}{\lambda_f}\cos(\theta_{m,k})\frac{\Delta x_{m,k}}{\Delta x_{m,k}^2+\Delta y_{m,k}^2}e^{-j\frac{2\pi\hbar_v^m d}{\lambda_f}\sin(\theta_{m,k})}. \quad (63)$$

Using the notations in (51), we can write

$$\frac{\partial \mathbf{r}_m[l_j]}{\partial \mathbf{T}_x^T} = \dot{\mathbf{C}}_m[l_j]\ , \quad (64)$$

but $\dot{\mathbf{a}}_m(l_j,\theta_{m,k})$ is computed by (62). Similarly, we have

$$\frac{\partial \mathbf{r}_m[l_j]}{\partial \mathbf{T}_y^T} = \dot{\mathbf{C}}_m[l_j]\ , \quad (65)$$

with $\dot{\mathbf{a}}_m(l_j,\theta_{m,k})$ computed by (63).

Substituting (64), (65), (52), (53) and (43) into (42), and then the near-field CRB can be calculated by (54).

Similarly, following the derivation steps in the far-field case, we can obtain the closed-form CRB expression for DOAs alone in the near-field case which also fits into (59), whereas the matrix $\mathbf{G}$ in (58) is updated to

$$\mathbf{G} = \tilde{\mathbf{W}}[\tilde{\dot{\mathbf{C}}}_x, \tilde{\dot{\mathbf{C}}}_y]\ . \quad (66)$$

Here, $\tilde{\dot{\mathbf{C}}}_x$ and $\tilde{\dot{\mathbf{C}}}_y$ are similarly defined as $\tilde{\dot{\mathbf{C}}}$ in (56), but their corresponding submatrices are replaced by (64) and (65), respectively.

VI. Simulation Results

In this section, as a comparison, the direct grid search method is employed for the MLE to minimize the total errors of the noise-corrupted angle measurements among all distributed platforms under the least square sense, where all the potential source locations are tried for the best fit of the measurements. The optimization problems of GS-SRACV in (25) and the GS-Localization (37) are solved using a software package called CVX [74], and the allowable error bound ε is chosen to give the best estimation results through trial-and-error in every experiment [1]. For comparison among different estimation methods, focusing is applied as a pre-processing step for the wideband signals and the actual incident angles are used for focusing without loss of generality.

A. DOA Estimation for Far-Field Sources

Consider an acoustic example, where a distributed sensor array network consisting of $M = 3$ sub-arrays placed on three receivers is employed, and each sub-array is a uniform linear array with $L_m = 6$ sensors, $\forall m = 1,2,3$. The frequency range of interest is from 7.5 kHz to 10 kHz with the reference frequency $f_r = 8.75$ kHz at the center frequency, and the normalized frequencies with a sampling frequency $f_s = 20$ kHz cover the range from 0.75π to π. The adjacent sensor spacing in each sub-array is $d = \lambda_r/2$, where λ_r is the wavelength corresponding to the reference frequency, the signal propagation speed $c = 340$ m/s, and DFT of $L = 64$ points is applied. The locations of the three sub-arrays are $\mathrm{U}_1(25,10)$, $\mathrm{U}_2(0,-50)$, and $\mathrm{U}_3(-70,90)$, while their rotation angles are 6°, 0°, and -21°, respectively. Here all the location coordinates are measured in metres. The spacings among the distributed platforms are 65.00 m, 124.20 m, and 156.52 m, respectively, and all of them are much larger than the largest signal wavelength $\lambda_{\max} = 0.0453$m. The propagation coefficients $b_{m,k}(t)$ are randomly generated constant complex values for all sub-arrays. Without loss of generality, we are interested in the far-field sources in front of the distributed sensor array network with the incident angles from -90° to 90° in this case. A search grid $\boldsymbol{\phi_g}$ including $K_g = 3601$ potential angles is generated within the full range with a step size of 0.05°.

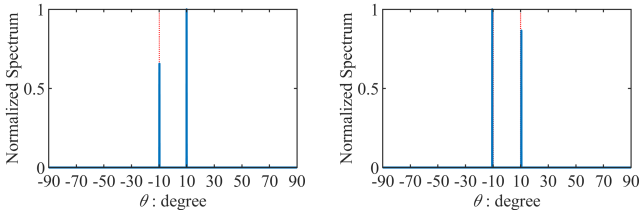

(a) Uncorrelated signals. (b) Coherent signals.

Fig. 5. DOA estimation results for two far-field sources.

For the first set of simulations, we consider the case of $K = 2$ far-field sources with incident angles of -10° and 10°, respectively. We set the input SNR as 0 dB and the number of snapshots is 1000. The DOA estimation results obtained by the proposed GS-SRACV method across all sub-arrays for uncorrelated impinging signals and coherent signals are shown in Fig. 5(a) and Fig. 5(b), respectively. It is clear that the incident angles of the two sources have been resolved successfully in both cases. In other words, the proposed method is capable of handling both uncorrelated and coherent signals.

For the next set of simulations, we take the uncorrelated case as an example and focus on the estimation performance by comparing the RMSE results of different methods. Fig. 6 gives the RMSE results with respect to input SNRs, where the number of snapshots is fixed at 1000. Then, we fix the SNR at 0 dB, and the RMSE results versus the number of snapshots are shown in Fig. 7. GS-SRACV (f_r) and MLE (f_r) represent the application of the GS-SRACV method and the MLE method based on a single frequency at f_r, respectively. GS-SRACV (f_r) performs better than the MLE (f_r), and the estimation accuracy of this single frequency case is the worst among all the three considered cases. The performances of the ℓ_1-SRACV method and the MUSIC method based on a single receiver (the first receiver located at U_1) are close to each other, with that of ℓ_1-SRACV a little better. Obviously, the proposed GS-SRACV and the MLE have outperformed the ℓ_1-SRACV and MUSIC by a big margin in both figures due to exploitation of the information acquired by the entire distributed sensor array network, with the best performance

[1] In [75], a suggested value is given to ensure the robustness of the global matched filter since it is challenging to obtain the optimal value of the regularization parameter. When the noise statistics are known or can be estimated in advance, the discrepancy principle can be employed to select the regularization parameter value and appropriate regularization parameter choices are provided for reasonably small noise levels [24]. Unfortunately, without prior knowledge of the source and noise statistics, and the source number, the choice of the regularization parameter is still an open problem [24], [25], [43], and ε is usually determined by simulation-based approach.

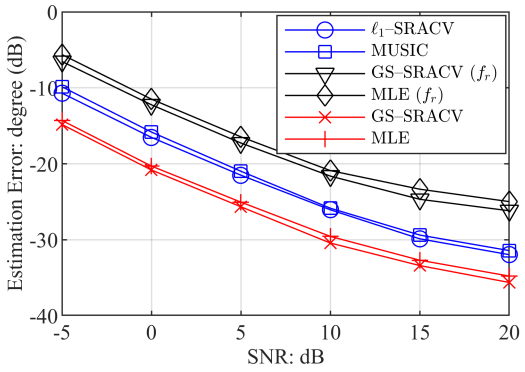

Fig. 6. RMSE versus input SNR for two far-field sources.

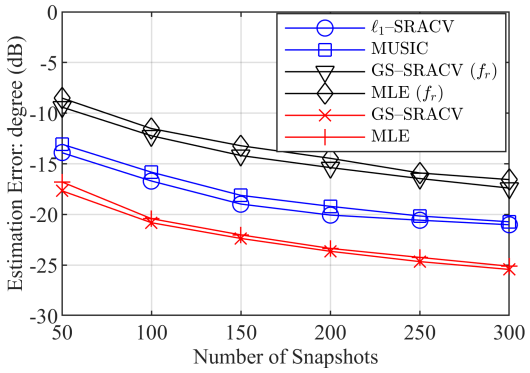

Fig. 7. RMSE versus number of snapshots for two far-field sources.

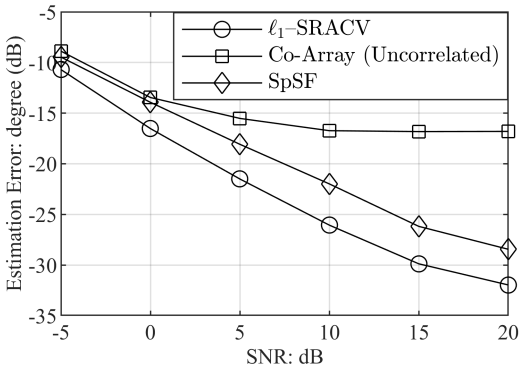

Fig. 8. RMSE versus input SNR for different Narrowband DOA estimation methods.

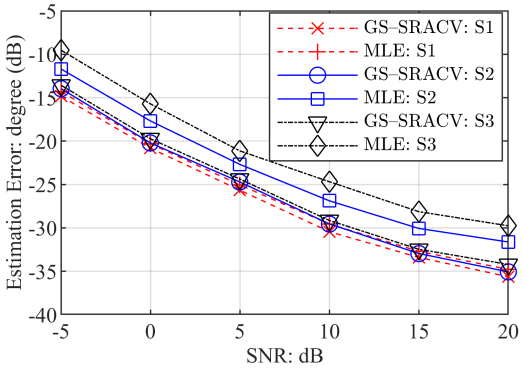

Fig. 9. RMSE versus input SNR for different scenarios in the far-field case.

achieved by the proposed GS-SRACV method.

The RMSE results obtained by the ℓ_1-SRACV, the co-array based method with *a priori* knowledge of uncorrelated sources where the vectorization process is conducted [32], [33], [36], [39], [43] (a special case of the SpSF method), and the SpSF method, are shown in Fig. 8. Clearly, in practice where the array output covariance matrix is estimated from the observed samples, the recovery of the approximated diagonal source covariance matrix in the co-array based method results in degradation in performance as verified in Fig. 8. The SpSF method outperforms the co-array based method, but its performance as well as computational complexity is still worse than the ℓ_1-SRACV method due to a more complicated optimization with significantly increased number of unknown parameters where the whole $K_g \times K_g$ entries of the source covariance matrix are to be optimized. Furthermore, the co-array based methods fail to deal with coherent sources.

Then, we consider two other scenarios by changing the rotation angle of the third sub-array. In Scenarios 2 (S2), the rotation angle of interest is set to $-41°$, while it is rotated by another $10°$ to $-51°$ in Scenarios 3 (S3). The RMSE results with respect to the input SNRs and the number of snapshots are given in Figs. 9 and 10, respectively, where the RMSE results of the above scenario 1, referred to as S1, are provided as a benchmark. Clearly, the performance of the MLE degrades significantly with the increase of the incident angle $\theta_{m,k}$ observed at the third sub-array (caused by the large rotation angle), while a better performance can always be obtained by our proposed GS-SRACV method.

Next, we further compare the RMSE results in different scenarios with the corresponding CRBs derived in Sec. V, as shown in Fig. 11. Obviously, the RMSE results of the proposed solution are close to the CRBs, while for sufficiently large input SNR with extremely low RMSE results, the estimation performance will be asymptotic to a constant due to the focusing approximation errors [46].

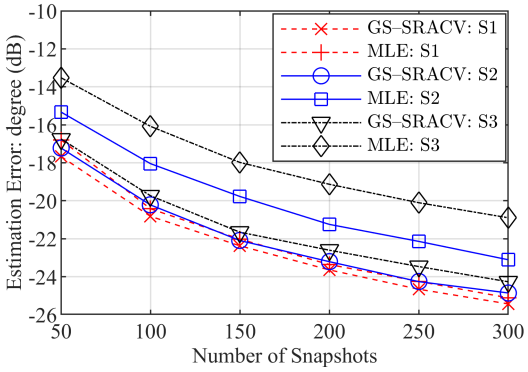

Fig. 10. RMSE versus number of snapshots for different scenarios in the far-field case.

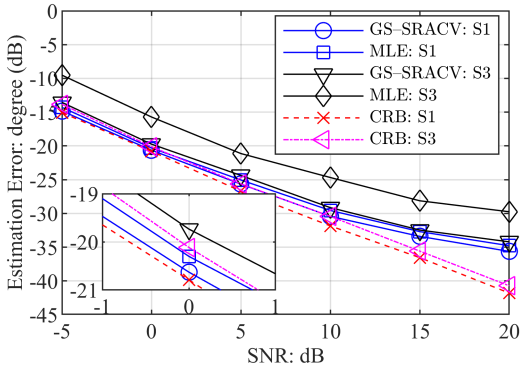

Fig. 11. Comparison between RMSE and CRB in the far-field case.

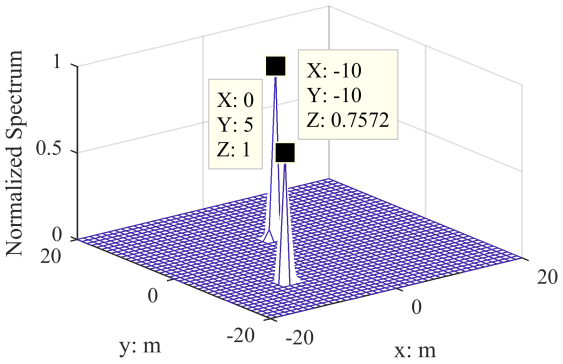

(a) Estimation results for the first step.

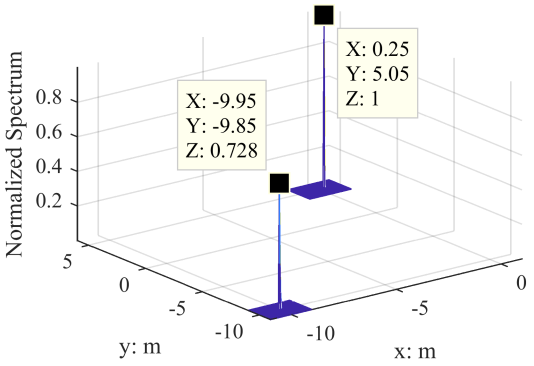

(b) Estimation results for the second step.

Fig. 12. Localization results for two near-field sources.

B. Localization for Near-Field Sources

We still consider the distributed sensor array network with $M = 3$ sub-arrays placed on the corresponding platforms, and the sub-array structure and the platform positions remain the same as in the previous setting. There are two sources considered in our simulations with positions $T_1(-10, -10)$ and $T_2(0, 5)$. The incident angles $\phi_{m,k}$ from the first source position to all the sub-arrays in the Cartesian coordinate system are $-119.74°$, $-14.04°$, and $149.04°$, while the incident angles from the second source are $-101.31°$, $0°$, and $140.53°$, respectively. With $\phi_{m_1,k} - \phi_{m_2,k} > 100°$ ($m_1 \neq m_2$, $m_1, m_2 = 1, 2, 3$), the sources should be considered as near-field ones. On the other hand, the sub-array aperture is $(L_m - 1)d \approx 0.1$ m, and therefore those sources are relatively far-field compared to each sub-array aperture. The rotation angles of the sub-arrays are set as $110°$, $0°$, and $-135°$, respectively, and the area of interest in the Cartesian coordinate system is $-20 \leq x \leq 20$ m and $-20 \leq y \leq 20$ m.

A two-step 2-D search grid refining strategy is used, where for the first step, a search grid with a larger step size of 1 m is considered within the full range of interest, i.e., the square area with $-20 \leq x \leq 20$ m and $-20 \leq y \leq 20$ m, while the search area is refined to $\tilde{x}_{T_k} - 1 \leq x \leq \tilde{x}_{T_k} + 1$ m and $\tilde{y}_{T_k} - 1 \leq y \leq \tilde{y}_{T_k} + 1$ m with a much smaller step size of 0.05 m in the second step, where $\tilde{T}_k(\tilde{x}_{T_k}, \tilde{y}_{T_k})$ is the detected source locations in the first step.

First, we fix the input SNR at 0 dB and the number of snapshots as 100. The localization results obtained by the proposed GS-Localization method is shown in Fig. 12, where the results for the first step with a larger step size is given in Fig. 12(a), while the results for the second step with a smaller step size is provided in Fig. 12(b), and the two peaks resolved represent the positions of the detected sources. We can see clearly that the detected source positions are very close to the actual source coordinates, which shows that the proposed method is capable of localizing the sources effectively. Similar to the far-field case, the proposed method is also capable of handling both uncorrelated and coherent signals.

In Figs. 13 and 14, we give the RMSE results of the different methods with respect to the input SNR and the number of snapshots, respectively. Clearly, the higher the input SNR or the number of snapshots, the higher its estimation accuracy. The proposed GS-Localization method is able to localize the sources over a wide range of input SNRs and number of snapshots with high accuracy, and offers better estimation results than the MLE for both the narrowband case (only the reference frequency bin is exploited for localization) and the wideband case. Furthermore, the estimation performance based on the wideband case outperforms the narrowband case consistently due to the exploitation of all the frequencies of interest. It is noted that for low input SNRs, the estimation accuracy of the angle measurements estimated independently at platforms decreases, and therefore worse localization results are obtained via MLE, which is easily affected by the bearings involved in the fusion procedure. However, in the proposed solution, the positions of the sources are calculated jointly with the involvement of the data collected by all sub-arrays, and thus outperforms the MLE consistently.

For the above simulations, focusing at actual DOAs is applied as a pre-processing step for wideband signals without loss of generality to make comparisons among different estimation methods. In Fig. 15, we further compare the performance of different focusing strategies, where the actual DOAs are used as the focusing angles for the ideal focusing case, while the iterative re-focused strategy in [46] is updated with refined grids centered by the estimated position $\tilde{T}_k^q(\tilde{x}_{T_k}^q, \tilde{y}_{T_k}^q)$ at the q-th iteration. Clearly, the performance employing the iterative re-focused strategy with two iterations (parameters remain the same as introduced at the beginning of Sec. V-B) is slightly worse than but close to the one with ideal

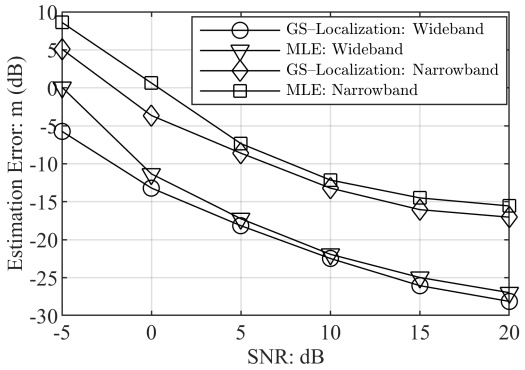

Fig. 13. RMSE versus input SNR for two near-field sources.

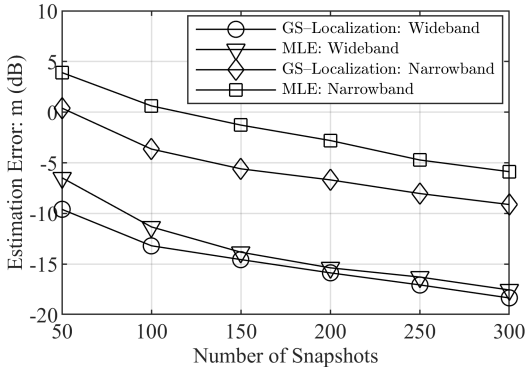

Fig. 14. RMSE versus number of snapshots for two near-field sources.

focusing angles. More iterations are required for high-accuracy estimation result with increased SNR.

Next, we consider two other scenarios by rotating the third sub-array at U_3. Compared with the aforementioned scenario, referred to as Scenario 1 (S1), we change the rotation angle of the third sub-array as -115° (Scenario 2, S2) and 105° (Scenario 3, S3), and then the incident angles $\theta_{3,k}$ of the two sources observed at the third sub-array become 34.04° and 25.53° in scenario 2, while they are 44.04° and 35.53° in scenario 3. The RMSE results versus the input SNRs and the number of snapshots are shown in Figs. 16 and 17, respectively. Obviously, for the same scenario, the proposed GS-

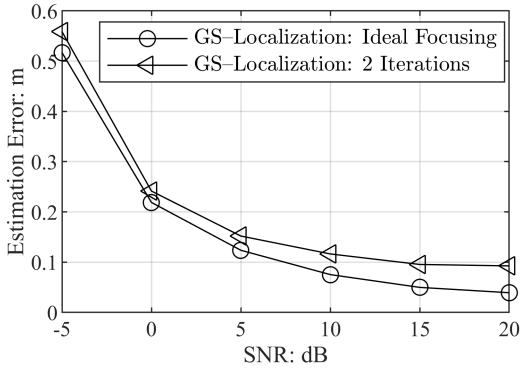

Fig. 15. RMSE versus input SNR for different focusing strategies.

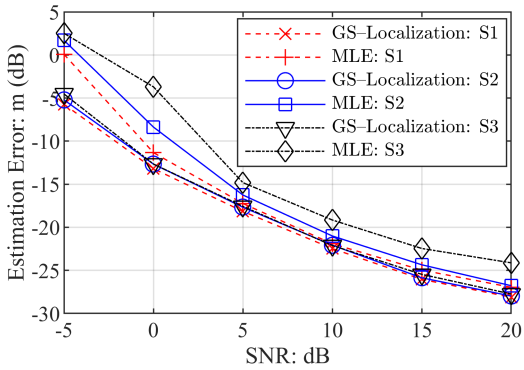

Fig. 16. RMSE versus input SNR for different scenarios in the near-field case.

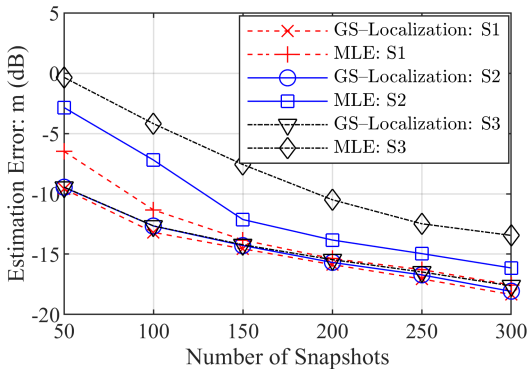

Fig. 17. RMSE versus number of snapshots for different scenarios in the near-field case.

Localization method outperforms the MLE. Furthermore, the performance of the MLE degrades sharply compared with the previous scenario due to the worse angle estimation involved in the final fusion process caused by the relatively large incident angle of the sources observed at the corresponding sub-array. Therefore, the performance of the MLE is sensitive to the angle measurements. On the contrary, better localization results are achieved for all scenarios by our proposed GS-Localization solution with all the information collected by the entire network processed as a whole.

Fig. 18 shows the RMSE results and the derived CRBs with respect to input SNRs. Similar to the far-field case, the RMSE results of the proposed localization method are close to the corresponding CRBs, while for sufficiently large input SNR with extremely low RMSE results, the estimation performance will be asymptotic to a constant due to the focusing approximation errors [46].

In summary, platforms providing worse angle measurements can spoil the overall performance of the MLE, while the proposed GS-Localization method can still achieve good estimation results in the same scenario. Overall, the GS-Localization method is a more effective solution to the localization problem.

VII. Conclusions

In this paper, the source localization problem based on a distributed sensor array network consisting of sub-arrays has

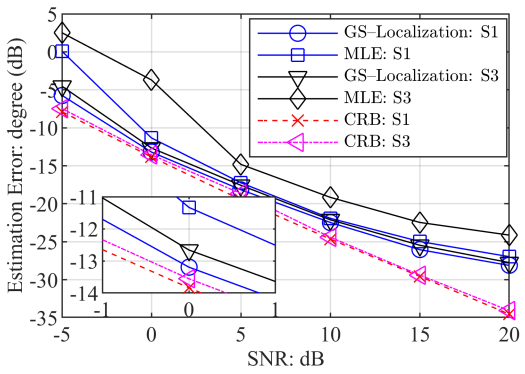

Fig. 18. Comparison between RMSE and CRB in the near-field case.

been studied. After the applications of DFT and focusing to deal with the wideband signals, the far-field sources were first considered, and a CS-based estimation method employing the group sparsity concept was proposed for DOA estimation by exploiting all the information collected by distributed platforms simultaneously. Then the near-field case (near-field compared to the whole distributed sensor array network, and still far-field from each sub-array perspective) was studied, and a group sparsity based 2-D localization method was proposed to localize the sources in the 2-D Cartesian coordinate system. It is noted that only the covariance matrix at each sub-array in lieu of all the data samples is required for centralized processing, and therefore the increase of the data exchange workload among platforms is limited. It has been shown by simulations that the proposed DOA estimation method for far-field sources and the localization method for near-field sources outperform the existing MLE consistently, and are more effective than the MLE, especially for the cases where some of the individual sub-array estimation results are not reliable.

For the localization problem of widely spread wideband sources, where the DOA of each source is not a single value, but spread over a continuous area centered to some assumed angle/location, the proposed approach is not designed and will not work for such a scenario and a different signal model is needed. We will further investigate this scenario in our future research work.

REFERENCES

[1] Q. Shen, W. Liu, L. Wang, and Y. Liu, "Group sparsity based target localization for distributed sensor array networks," in *Proc. IEEE International Conference on Acoustics, Speech, and Signal Processing (ICASSP)*, Brighton, UK, May 2019, pp. 4190–4194.

[2] M. Gavish and A. J. Weiss, "Performance analysis of bearing-only target location algorithms," *IEEE Trans. Aerosp. Electron. Syst.*, vol. 28, no. 3, pp. 817–828, Jul. 1992.

[3] G. Destino and G. Abreu, "On the maximum likelihood approach for source and network localization," *IEEE Trans. Signal Process.*, vol. 59, no. 10, pp. 4954–4970, Oct. 2011.

[4] G. Mao, B. Fidan, and B. D. Anderson, "Wireless sensor network localization techniques," *Computer networks*, vol. 51, no. 10, pp. 2529–2553, 2007.

[5] C. Liu, D. Fang, Z. Yang, H. Jiang, X. Chen, W. Wang, T. Xing, and L. Cai, "RSS distribution-based passive localization and its application in sensor networks," *IEEE Trans. Wireless Commun.*, vol. 15, no. 4, pp. 2883–2895, Apr. 2016.

[6] I. Guvenc and C.-C. Chong, "A survey on TOA based wireless localization and nlos mitigation techniques," *IEEE Communications Surveys & Tutorials*, vol. 11, no. 3, Aug. 2009.

[7] Y. Wang and K. Ho, "An asymptotically efficient estimator in closed-form for 3-D AOA localization using a sensor network," *IEEE Trans. Wireless Commun.*, vol. 14, no. 12, pp. 6524–6535, Dec. 2015.

[8] L. M. Kaplan, Q. Le, and N. Molnar, "Maximum likelihood methods for bearings-only target localization," in *Proc. IEEE International Conference on Acoustics, Speech, and Signal Processing (ICASSP)*, vol. 5. IEEE, 2001, pp. 3001–3004.

[9] T. Lv, F. Tan, H. Gao, and S. Yang, "A beamspace approach for 2-D localization of incoherently distributed sources in massive MIMO systems," *Signal Processing*, vol. 121, pp. 30–45, 2016.

[10] N. Garcia, H. Wymeersch, E. G. Larsson, A. M. Haimovich, and M. Coulon, "Direct localization for massive MIMO," *IEEE Trans. Signal Process.*, vol. 65, no. 10, pp. 2475–2487, May 2017.

[11] H.-J. Shao, X.-P. Zhang, and Z. Wang, "Efficient closed-form algorithms for AOA based self-localization of sensor nodes using auxiliary variables." *IEEE Trans. Signal Process.*, vol. 62, no. 10, pp. 2580–2594, 2014.

[12] Y. Wang and K. Ho, "Unified near-field and far-field localization for AOA and hybrid AOA-TDOA positionings," *IEEE Trans. Wireless Commun.*, vol. 17, no. 2, pp. 1242–1254, Feb. 2018.

[13] Y.-D. Huang and M. Barkat, "Near-field multiple source localization by passive sensor array," *IEEE Trans. Antennas Propag.*, vol. 39, no. 7, pp. 968–975, Jul. 1991.

[14] Q. Shen, W. Liu, W. Cui, and S. Wu, "Underdetermined DOA estimation under the compressive sensing framework: A review," *IEEE Access*, vol. 4, pp. 8865–8878, 2016.

[15] J. Liang and D. Liu, "Passive localization of near-field sources using cumulant," *IEEE Sensors Journal*, vol. 9, no. 8, pp. 953–960, 2009.

[16] N. Patwari, J. N. Ash, S. Kyperountas, A. O. Hero, R. L. Moses, and N. S. Correal, "Locating the nodes: cooperative localization in wireless sensor networks," *IEEE Signal Process. Mag.*, vol. 22, no. 4, pp. 54–69, 2005.

[17] C. Elkin, R. Kumarasiri, D. B. Rawat, and V. Devabhaktuni, "Localization in wireless sensor networks: A dempster-shafer evidence theoretical approach," *Ad Hoc Networks*, vol. 54, pp. 30–41, 2017.

[18] R. O. Schmidt, "Multiple emitter location and signal parameter estimation," *IEEE Trans. Antennas Propag.*, vol. 34, no. 3, pp. 276–280, Mar. 1986.

[19] R. Roy and T. Kailath, "ESPRIT-estimation of signal parameters via rotational invariance techniques," *IEEE Trans. Acoust., Speech, Signal Process.*, vol. 37, no. 7, pp. 984–995, Jul. 1989.

[20] W. Du and R. L. Kirlin, "Improved spatial smoothing techniques for DOA estimation of coherent signals," *IEEE Trans. Signal Process.*, vol. 39, no. 5, pp. 1208–1210, May 1991.

[21] D. L. Donoho, "Compressed sensing," *IEEE Trans. Inf. Theory*, vol. 52, no. 4, pp. 1289 – 1306, 2006.

[22] P. Stoica, P. Babu, and J. Li, "SPICE: A sparse covariance-based estimation method for array processing," *IEEE Trans. Signal Process.*, vol. 59, no. 2, pp. 629–638, Feb. 2011.

[23] Q. Shen, W. Liu, W. Cui, and S. Wu, "Low-complexity compressive sensing based DOA estimation for co-prime arrays," in *Proc. International Conference on Digital Signal Processing (DSP)*, Hong Kong, China, Aug. 2014, pp. 754–758.

[24] D. Malioutov, M. Çetin, and A. S. Willsky, "A sparse signal reconstruction perspective for source localization with sensor arrays," *IEEE Trans. Signal Process.*, vol. 53, no. 8, pp. 3010–3022, Aug. 2005.

[25] J. Yin and T. Chen, "Direction-of-arrival estimation using a sparse representation of array covariance vectors," *IEEE Trans. Signal Process.*, vol. 59, no. 9, pp. 4489–4493, Sep. 2011.

[26] G. Tang and A. Nehorai, "Performance analysis for sparse support recovery," *IEEE Trans. Inf. Theory*, vol. 56, no. 3, pp. 1383–1399, Mar. 2010.

[27] A. Koochakzadeh, H. Qiao, and P. Pal, "On fundamental limits of joint sparse support recovery using certain correlation priors," *IEEE Trans. Signal Process.*, vol. 66, no. 17, pp. 4612–4625, 2018.

[28] H. Qiao and P. Pal, "Guaranteed localization of more sources than sensors with finite snapshots in multiple measurement vector models using difference co-arrays," *IEEE Trans. Signal Process.*, vol. 67, no. 22, pp. 5715–5729, 2019.

[29] Y. Jin and B. Rao, "Support recovery of sparse signals in the presence of multiple measurement vectors," *IEEE Trans. Inf. Theory*, vol. 59, no. 5, pp. 3139–3157, 2013.

[30] Z. Yang and L. Xie, "Exact joint sparse frequency recovery via optimization methods," *IEEE Trans. Signal Process.*, vol. 64, no. 19, pp. 5145–5157, 2016.

[31] C. Steffens, M. Pesavento, and M. E. Pfetsch, "A compact formulation for the $ell_{2,1}$ mixed-norm minimization problem," *IEEE Trans. Signal Process.*, vol. 66, no. 6, pp. 1483–1497, 2018.

[32] J. Zheng and M. Kaveh, "Sparse spatial spectral estimation: a covariance fitting algorithm, performance and regularization," *IEEE Trans. Signal Process.*, vol. 61, no. 11, pp. 2767–2777, Jun. 2013.

[33] B. Ottersten, P. Stoica, and R. Roy, "Covariance matching estimation techniques for array signal processing applications," *Digital Signal Processing*, vol. 8, no. 3, pp. 185–210, 1998.

[34] Y. D. Zhang, M. G. Amin, and B. Himed, "Sparsity-based DOA estimation using co-prime arrays," in *Proc. IEEE International Conference on Acoustics, Speech and Signal Processing (ICASSP)*, Vancouver, Canada, May 2013, pp. 3967–3971.

[35] Q. Shen, W. Liu, W. Cui, and S. Wu, "Extension of nested arrays with the fourth-order difference co-array enhancement," in *Proc. IEEE International Conference on Acoustics, Speech and Signal Processing (ICASSP)*, Shanghai, China, Mar. 2016, pp. 2991–2995.

[36] S. Qin, Y. D. Zhang, and M. G. Amin, "Generalized coprime array configurations for direction-of-arrival estimation," *IEEE Transactions on Signal Processing*, vol. 63, no. 6, pp. 1377–1390, March 2015.

[37] Q. Shen, W. Liu, W. Cui, and S. Wu, "Extension of co-prime arrays based on the fourth-order difference co-array concept," *IEEE Signal Process. Lett.*, vol. 23, no. 5, pp. 615–619, May 2016.

[38] A. Raza, W. Liu, and Q. Shen, "Thinned coprime array for second-order difference co-array generation with reduced mutual coupling," *IEEE Trans. Signal Process.*, vol. 67, no. 8, pp. 2052–2065, 2019.

[39] Q. Shen, W. Liu, W. Cui, S. Wu, and P. Pal, "Simplified and enhanced multiple level nested arrays exploiting high-order difference co-arrays," *IEEE Trans. Signal Process.*, vol. 67, no. 13, pp. 3502–3515, Jul. 2019.

[40] G. Su and M. Morf, "The signal subspace approach for multiple wide-band emitter location," *IEEE Trans. Acoust., Speech, Signal Process.*, vol. 31, no. 6, pp. 1502–1522, Dec. 1983.

[41] H. Wang and M. Kaveh, "Coherent signal-subspace processing for the detection and estimation of angles of arrival of multiple wide-band sources," *IEEE Trans. Acoust., Speech, Signal Process.*, vol. 33, no. 4, pp. 823–831, Aug. 1985.

[42] Y.-S. Yoon, L. M. Kaplan, and J. H. McClellan, "TOPS: new DOA estimator for wideband signals," *IEEE Trans. Signal Process.*, vol. 54, no. 6, pp. 1977–1989, Jun. 2006.

[43] Q. Shen, W. Liu, W. Cui, S. Wu, Y. D. Zhang, and M. G. Amin, "Low-complexity direction-of-arrival estimation based on wideband co-prime arrays," *IEEE/ACM Trans. Audio, Speech, Language Process.*, vol. 23, no. 9, pp. 1445–1456, Sep. 2015.

[44] Q. Shen, W. Cui, W. Liu, S. Wu, Y. D. Zhang, and M. G. Amin, "Under-determined wideband DOA estimation of off-grid sources employing the difference co-array concept," *Signal Processing*, vol. 130, pp. 299–304, 2017.

[45] Q. Shen, W. Liu, W. Cui, S. Wu, Y. D. Zhang, and M. G. Amin, "Focused compressive sensing for underdetermined wideband DOA estimation exploiting high-order difference coarrays," *IEEE Signal Process. Lett.*, vol. 24, no. 1, pp. 86–90, Jan. 2017.

[46] W. Cui, Q. Shen, W. Liu, and S. Wu, "Low complexity DOA estimation for wideband off-grid sources based on re-focused compressive sensing with dynamic dictionary," *IEEE Journal of Selected Topics in Signal Processing*, vol. 13, no. 5, pp. 918–930, Sep. 2019.

[47] M. Pesavento, A. B. Gershman, and K. M. Wong, "Direction finding in partly calibrated sensor arrays composed of multiple subarrays," *IEEE Trans. Signal Process.*, vol. 50, no. 9, pp. 2103–2115, 2002.

[48] P. Parvazi, M. Pesavento, and A. B. Gershman, "Direction-of-arrival estimation and array calibration for partly-calibrated arrays," in *Proc. IEEE International Conference on Acoustics, Speech, and Signal Processing (ICASSP)*. IEEE, 2011, pp. 2552–2555.

[49] P. Stoica, A. Nehorai, and T. Söderström, "Decentralized array processing using the MODE algorithm," *Circuits, Systems and Signal Processing*, vol. 14, no. 1, pp. 17–38, 1995.

[50] C. M. S. See and A. B. Gershman, "Direction-of-arrival estimation in partly calibrated subarray-based sensor arrays," *IEEE Trans. Signal Process.*, vol. 52, no. 2, pp. 329–338, 2004.

[51] D. W. Rieken and D. R. Fuhrmann, "Generalizing MUSIC and MVDR for multiple noncoherent arrays," *IEEE Trans. Signal Process.*, vol. 52, no. 9, pp. 2396–2406, 2004.

[52] W. Suleiman and P. Parvazi, "Search-free decentralized direction-of-arrival estimation using common roots for non-coherent partly calibrated arrays," in *Proc. IEEE International Conference on Acoustics, Speech, and Signal Processing (ICASSP)*. IEEE, 2014, pp. 2292–2296.

[53] F. Wen, Q. Wan, R. Fan, and H. Wei, "Improved MUSIC algorithm for multiple noncoherent subarrays," *IEEE Signal Process. Lett.*, vol. 21, no. 5, pp. 527–530, 2014.

[54] T. Tirer and O. Bialer, "Effective approximate maximum likelihood estimation of angles of arrival for non-coherent sub-arrays," in *Proc. IEEE International Conference on Acoustics, Speech, and Signal Processing (ICASSP)*. IEEE, 2020, pp. 4557–4561.

[55] C. Reyes, T. Hilaire, and C. F. Mecklenbräuker, "Distributed projection approximation subspace tracking based on consensus propagation," in *Proc. IEEE International Workshop on Computational Advances in Multi-Sensor Adaptive Processing (CAMSAP)*. IEEE, 2009, pp. 340–343.

[56] L. Li, A. Scaglione, and J. H. Manton, "Distributed principal subspace estimation in wireless sensor networks," *IEEE Journal of Selected Topics in Signal Processing*, vol. 5, no. 4, pp. 725–738, 2011.

[57] W. Suleiman, M. Pesavento, and A. Zoubir, "Decentralized direction finding using partly calibrated arrays," in *Proc. European Signal Processing Conference (EUSIPCO)*. IEEE, 2013, pp. 1–5.

[58] W. Suleiman, P. Parvazi, M. Pesavento, and A. M. Zoubir, "Non-coherent direction-of-arrival estimation using partly calibrated arrays," *IEEE Trans. Signal Process.*, vol. 66, no. 21, pp. 5776–5788, 2018.

[59] Z. Wang, J.-A. Luo, and X.-P. Zhang, "A novel location-penalized maximum likelihood estimator for bearing-only target localization," *IEEE Trans. Signal Process.*, vol. 60, no. 12, pp. 6166–6181, Dec. 2012.

[60] C. Wang, F. Qi, G. Shi, and X. Wang, "Convex combination based target localization with noisy angle of arrival measurements," *IEEE Wireless Communication Letters*, vol. 3, no. 1, pp. 14–17, Feb. 2014.

[61] T. Erseghe, "A distributed and maximum-likelihood sensor network localization algorithm based upon a nonconvex problem formulation," *IEEE Transactions on Signal and Information Processing over Networks*, vol. 1, no. 4, pp. 247–258, Dec. 2015.

[62] J.-P. Le Cadre and C. Jaetffret, "On the convergence of iterative methods for bearings-only tracking," *IEEE Trans. Aerosp. Electron. Syst.*, vol. 35, no. 3, pp. 801–818, Jul. 1999.

[63] K. Dogancay, "Bias compensation for the bearings-only pseudolinear target track estimator," *IEEE Trans. Signal Process.*, vol. 54, no. 1, pp. 59–68, Jan. 2006.

[64] Q. Shen, W. Liu, L. Wang, and Y. Liu, "Adaptive beamforming for target detection and surveillance based on distributed unmanned aerial vehicle platforms," *IEEE Access*, vol. 6, pp. 60 812–60 823, 2018.

[65] C. Wann, "Mobile sensing systems based on improved gdop for target localization and tracking," in *Proc. IEEE SENSORS*, 2012, pp. 1–4.

[66] H. Hung and M. Kaveh, "Focussing matrices for coherent signal-subspace processing," *IEEE Trans. Acoust., Speech, Signal Process.*, vol. 36, no. 8, pp. 1272–1281, Aug. 1988.

[67] D. N. Swingler and J. Krolik, "Source location bias in the coherently focused high-resolution broad-band beamformer," *IEEE transactions on acoustics, speech, and signal processing*, vol. 37, no. 1, pp. 143–145, 1989.

[68] S. Valaee and P. Kabal, "The optimal focusing subspace for coherent signal subspace processing," *IEEE Trans. Signal Process.*, vol. 44, no. 3, pp. 752–756, 1996.

[69] P. M. Schultheiss and H. Messer, "Optimal and suboptimal broad-band source location estimation," *IEEE Trans. Signal Process.*, vol. 41, no. 9, pp. 2752–2763, 1993.

[70] Y. Liang, Q. Shen, W. Cui, and W. Liu, "Cramér-rao bound for wideband DOA estimation with uncorrelated sources," in *Proc. IEEE Global Conference on Signal and Information Processing (GlobalSIP)*, 2019.

[71] R. A. Fisher, "On the mathematical foundations of theoretical statistics," *Philosophical Transactions of the Royal Society of London, Series A*, vol. 222, pp. 309–368, 1922.

[72] P. Stoica, E. G. Larsson, and A. B. Gershman, "The stochastic CRB for array processing: A textbook derivation," *IEEE Signal Process. Lett.*, vol. 8, no. 5, pp. 148–150, 2001.

[73] P. Stoica and R. L. Moses, *Spectral Analysis of Signals*. Upper Saddle River, NJ, USA: Pearson Prentice Hall, 2005.

[74] M. Grant and S. Boyd. (2013, Dec.) CVX: Matlab software for disciplined convex programming, version 2.0 beta, build 1023. [Online]. Available: http://cvxr.com/cvx

[75] J.-J. Fuchs, "On the application of the global matched filter to DOA estimation with uniform circular arrays," *IEEE Trans. Signal Process.*, vol. 49, no. 4, pp. 702–709, 2001.

Qing Shen received his B.S. degree in 2009 and Ph.D. degree in 2016, both from the Beijing Institute of Technology, Beijing, China. He then worked as a Postdoctoral Researcher with the Beijing Institute of Technology, where he is currently an Associate Professor. From 2013 to 2015 and from 2018 to 2019, he was a Sponsored Researcher with the Department of Electronic and Electrical Engineering, University of Sheffield, Sheffield, UK. His research interests include sensor array signal processing, and its various applications such as acoustics, radar, sonar, and wireless communications. He was the recipient of two Excellent Ph.D. Thesis Awards from both the Chinese Institute of Electronics and the Beijing Institute of Technology in 2016. He was also the recipient of the Second-Class Prize of the National Award for Technological Invention in 2019, the First-Class Prize of the Science and Technology (Technological Invention) Award from the Chinese Institute of Electronics in 2018, and the Second-Class Prize of the Ministerial Level Science and Technology Progress Award in 2014.

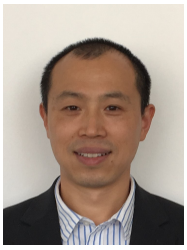

Wei Liu (S'01-M'04-SM'10) received his BSc and LLB. degrees from Peking University, China, in 1996 and 1997, respectively, MPhil from the University of Hong Kong in 2001, and PhD from the School of Electronics and Computer Science, University of Southampton, UK, in 2003. He then worked as a postdoc first at Southampton and later at the Department of Electrical and Electronic Engineering, Imperial College London. Since September 2005, he has been with the Department of Electronic and Electrical Engineering, University of Sheffield, UK, first as a Lecturer and then a Senior Lecturer. He has published more than 300 journal and conference papers, five book chapters, and two research monographs titled "Wideband Beamforming: Concepts and Techniques" (John Wiley, March 2010) and "Low-Cost Smart Antennas" (by Wiley-IEEE, March 2019), respectively. His research interests cover a wide range of topics in signal processing, with a focus on sensor array signal processing and its various applications, such as robotics and autonomous systems, human computer interface, radar, sonar, satellite navigation, and wireless communications.

He is a member of the Digital Signal Processing Technical Committee of the IEEE Circuits and Systems Society (Secretary from 2020) and the Sensor Array and Multichannel Signal Processing Technical Committee of the IEEE Signal Processing Society (Vice-Chair from Jan 2019). He was an Associate Editor for IEEE Trans. on Signal Processing (March 2015-March 2019) and is currently an Associate Editor for IEEE Access, and an editorial board member of the Journal Frontiers of Information Technology and Electronic Engineering.

Li Wang received his B.Sc. and M.Sc. degrees in Electronic and Electrical Engineering from the University of Electronic Science and Technology of China, Chengdu, China, in 2000 and 2008, respectively. He is currently pursuing his Ph.D. degree in Sichuan University, Chengdu, China. He is the director of the Key Laboratory, Southwest China Institute of Electronic Technology. His research interests include distributed array signal processing and adaptive signal processing.

Yin Liu received his B.Sc., M.Sc. and Ph.D. degrees in electronic engineering from Xidian University, Xi'an, China, in 2002, 2005 and 2012, respectively. He is a researcher at the Southwest China Institute of Electronic Technology. He was a visiting researcher at the University of Sheffield sponsored by the China Scholarship Council. His research interests include array signal processing, sparse signal recovery, and MIMO radar signal processing.